INSTITUTE OF PHYSICS PUBLISHING SUPERCONDUCTOR SCIENCE AND TECHNOLOGY

Supercond. Sci. Technol. **14** (2001) R53–R77 www.iop.org/Journals/su PII: S0953-2048(01)01568-8

TOPICAL REVIEW

Andreev bound states in high-T_c superconducting junctions

T Löfwander, V S Shumeiko and G Wendin

Department of Microelectronics and Nanoscience, School of Physics and Engineering Physics, Chalmers University of Technology and Göteborg University, S-412 96 Göteborg, Sweden

Received 12 June 2000, in final form 9 January 2001

Abstract

The formation of bound states at surfaces of materials with an energy gap in the bulk electron spectrum is a well known physical phenomenon. At superconductor surfaces, quasiparticles with energies inside the superconducting gap Δ may be trapped in bound states in quantum wells, formed by total reflection against the vacuum and total Andreev reflection against the superconductor. Since an electron reflects as a hole and sends a Cooper pair into the superconductor, the surface states give rise to resonant transport of quasiparticle and Cooper pair currents, and may be observed in tunnelling spectra. In superconducting junctions these surface states may hybridize and form bound Andreev states, trapped between the superconducting electrodes. In d-wave superconductors, the order parameter changes sign under 90° rotation and, as a consequence, Andreev reflection may lead to the formation of zero energy quasiparticle bound states, midgap states (MGS). The formation of MGS is a robust feature of d-wave superconductivity and provides a unified framework for many important effects which will be reviewed: large Josephson current, low-temperature anomaly of the critical Josephson current, π-junction behaviour, $0 \rightarrow \pi$ junction crossover with temperature, zero-bias conductance peaks, paramagnetic currents, time reversal symmetry breaking, spontaneous interface currents, and resonance features in subgap currents. Taken together these effects, when observed in experiments, provide proof for d-wave superconductivity in the cuprates.

Contents

1. Introduction

Ever since the discovery of high-T_c superconductivity (Bednorz and Müller 1986) spin-fluctuation mediated d-wave singlet pairing has been a major candidate for superconductive pairing in the cuprates (Dagotto 1994, Scalapino 1995). From the start it was realized that the layered cuprates are low-dimensional systems with antiferromagnetic undoped parent compounds, with strong electron correlations and with highly unusual normal electron properties. Nevertheless, phonon-mediated strong-coupling s-wave singlet pairing could not be ruled out because of the experimental difficulty in identifying essential d-wave signatures, which cannot be explained within an s-wave picture. Looking back, it seems that the essential quantitative body of facts, not directly addressing the qualitative question of symmetry, was already known by 1990. In particular, one early experimental result may be regarded as a clear qualitative signature of d-wave pairing: the so-called zero-bias conductance peak (ZBCP) observed in the I–V characteristics of electron tunnelling into thin films of YBaCaCuO by Geerk *et al* (1988). However, the d-wave connection was not realized at the time; it was later proposed by Hu (1994) and Kashiwaya *et al* (1995) and then experimentally verified by Covington *et al* (1997) in a study of the magnetic field dependence of the splitting of the ZBCP.

A great deal of effort has gone into finding the most significant evidence for d-wave pairing symmetry of the order parameter in the high-T_c cuprates (see, for example, the review papers by Dagotto (1994), Scalapino (1995) and Annett *et al* (1996) and references therein). The problem is non-trivial because it is necessary to distinguish d-wave symmetry from anisotropic s-wave symmetry. A d-wave order parameter has nodes at four mutually perpendicular directions of the electron momentum. This provides gapless superconductivity in the direction of the nodes, with normal excitations existing at all energies, having far-reaching consequences for the material properties of the superconducting state, for example linear heat capacity at low temperature, large subgap tunnel current, smeared gap structures, and high sensitivity to non-magnetic impurities. These properties have indeed been found in experiments, from the beginning. Moreover, anisotropic gap structures with deep minima in the node directions have been established in angle resolved photoemission experiments. The problem is, however, that these experimental facts are also consistent with an anisotropic s-wave order parameter (see the review by Annett *et al* (1996) for an analysis of experimental results).

To make an '*experimentum crucius*' one has to establish that the order parameter *changes sign* when the momentum rotates by 90°. Such experiments have earlier been suggested by Geshkenbein *et al* (1987) in connection with heavy fermion superconductivity, and first realized in tunnelling experiments on high-T_c superconductors by Wollman *et al* (1993). The idea behind these experiments is based on the phase sensitive properties of Josephson junctions involving d-wave and s-wave, or two misoriented d-wave, superconducting electrodes. When the junction electrodes have different signs of the order parameter, this is equivalent to adding a π-shift to the superconducting phase difference across the junction, and therefore the stable state of the junction corresponds to a superconducting phase difference equal to $\phi = \pi$ (π-junctions), instead of $\phi = 0$, as in conventional junctions.

The conceptually simplest way to create a π-junction is to attach a superconducting loop to two adjacent faces at right angles of a high-T_c single crystal, creating a SQUID circuit with one π-junction (Mathai *et al* 1995, Wollman *et al* 1995, van Harlingen 1995, Schulz *et al* 2000). Using tri-crystal substrates one can create a superconducting ring consisting of an odd number of π-junctions, which is able to trap half-integer flux quanta. This was studied by Tsuei *et al* (1994, 1996, 1997) and Kirtley *et al* (1995b, 1996) who used a scanning SQUID to detect spontaneous half-integer flux quanta in the π-junction loop but no flux quanta in rings on bi-crystal interfaces; for an overview of the subject, see the recent review article by Tsuei and Kirtley (2000a). This is in principle the definitive experiment, but it is desirable that it can be repeated by other groups.

There is however another type of experiment which may provide direct evidence for d-wave symmetry of the order parameter. These experiments exploit the property of the d-wave superconductors to form superconducting bound surface states at the Fermi energy, so-called midgap states (MGS) (Hu 1994). A MGS is a direct consequence of the angle-dependent sign change of the order parameter, and it cannot exist in s-wave superconductors. Transport measurements which detect the MGS resonance at the Fermi energy for particular orientations of the plane of the junction with respect to the crystallographic axes will provide crucial evidence for d-wave superconductivity.

The problem of MGS is part of a general problem of superconducting surface and interface states and their relation to the Andreev states, which determine the transport properties of superconducting junctions. This is the topic of the present review.

2. Superconducting surface states

As is well known, at semiconductor and metal surfaces quasiparticle surface states may exist in the band gaps of the bulk material (see, for example, Ashcroft and Mermin 1976). The situation is similar at a superconductor surface; the important difference is, however, that on a superconductor surface, electrons are reflected as holes and holes are reflected as electrons—Andreev reflection (Andreev 1964)—while on a normal surface electrons are reflected in the normal way as electrons.

Superconducting quasiparticle surface states were first described by de Gennes and Saint-James (1963) for the insulator-normal metal-superconductor (INS) quantum well. More recently it was found that the superconducting surface states do not need a normal region at the surface and they exist at an arbitrary interface between an s-wave superconductor and an insulator (Wendin and Shumeiko 1996a). The energy of the surface states lies within the energy gap of the superconductor and it depends on the properties of the surface. In d-wave superconductors, due to the specific symmetry of the order parameter, these levels may occur exactly at the Fermi energy (Hu 1994, 1998).

In superconducting junctions, the overlap of the wavefunctions of the surface states builds up stationary states

at certain energies, the Andreev bound states. These states are thus states of the entire junction, similar to bonding and antibonding states in a molecule or in a system of two closely separated metal surfaces. The name of these bound states are associated with Andreev, who first studied them in perfect superconductor-normal metal-superconductor (SNS) junctions (Andreev 1965). Due to their ability to carry current, the Andreev bound states play an essential role in dc Josephson transport (Kulik 1969, Bardeen and Johnson 1972). Moreover, the surface states in superconductor–normal metal and superconductor–superconductor junctions introduce resonances in the current transport under applied voltage bias.

2.1. Andreev reflection

An important aspect of the superconducting surface states is that they are built up from a combination of electron and hole wavefunctions. This mixing is induced by the specific property of the superconductor interface known as *Andreev reflection*.

The problem was originally raised by the observation of an anomalously large thermal resistance of superconductors in the intermediate state (Mendelssohn and Olsen 1950, Zavaritsky 1960). It was suggested that the enhancement of the thermal resistance was due to some strong additional quasiparticle scattering at the normal metal/superconductor (NS) interfaces (Hulm 1953, Strässler and Wyder 1963). However, no microscopic mechanism for such a reflection was proposed because the spatial variation of the order parameter in the intermediate state is smooth on the scale of the Fermi wavelength, and it was not clear how such a 'soft' potential could provide efficient electron reflection. The problem was solved by Andreev who showed that the reflection at NS interfaces is due to electron–hole conversion (Andreev 1964).

Let us consider a contact between a superconductor and a normal metal, and assume for simplicity that the normal electron properties of both electrodes are identical. This means that normal electrons will not be reflected by the contact—perfect transmission in the normal state. However, electrons in the normal electrode which approach the interface with an energy E inside the superconducting gap, $|E| < \Delta$, cannot penetrate into the superconducting electrode. At the same time, there is no normal scattering process at the interface which is able to reverse the electron momentum. The problem is solved by converting the incoming electron into a *reflected hole* moving with the *same momentum* in the opposite direction: since the hole energy is given by $E^h = E_F - p^2/2m$, the group velocity is $v^h = \mathrm{d}E^h/\mathrm{d}p \approx -v_F$. Such a conversion, Andreev reflection, occurs due to electron–hole correlations within the superconducting electrode.

A straightforward quantum mechanical analysis (see the appendix) shows that Andreev reflection is accompanied by a phase shift $-\gamma(E)\mp\chi$, where the upper sign corresponds to the conversion of an electron into a hole, and the lower sign to the inverse process. In this expression, $\gamma(E) = \arccos(E/|\Delta|)$ is the Andreev reflection phase shift and χ is the phase of the superconducting order parameter. The wavefunctions of the electrons and holes penetrate into the superconductor over a length of the order of the superconducting coherence length, $\xi_0 = \hbar v_F/\Delta$, and therefore the electron–hole conversion occurs over this distance. Thus, the phase shift during Andreev reflection is sensitive to the profile $\Delta(x)$ of the superconducting order parameter over a distance of the order of a coherence length near the interface. Calculation of this profile involves self-consistent treatment of the order parameter: however, the properties of the surface states can be qualitatively understood by replacing the exact form of $\Delta(x)$ by a step function $\Delta(x) = \Delta\Theta(x)$.

2.2. Surface states

Let us now consider the formation of superconducting bound states in an INS quantum well with a specular vacuum/metal (IN) interface surface. We will first consider a two-dimensional s-wave superconductor with anisotropic order parameter which has a perfectly transparent NS interface with a normal layer of width L, as shown in figure 1. According to quasiclassical arguments, the bound state corresponds to a closed quasiparticle trajectory, and the bound state energy is given by the Bohr–Sommerfeld quantization condition, which requires the total phase accumulated during one cycle to be equal to an integer number of 2π. The quasiparticle trajectory in figure 1 (corresponding to electron motion in the $+k_y$-direction) consists of an electron segment which includes a single reflection at the IN interface, and of a hole segment which retraces backwards the electron trajectory. The total accumulated phase consists of two parts: (i) a contribution from the Andreev reflections: $-\gamma - \chi$ in the θ-direction and $-\bar{\gamma} + \bar{\chi}$ in the $\bar{\theta}$-direction (θ is the angle between the electron trajectory and the surface normal and $\bar{\theta} = \pi - \theta$ is the angle after specular normal reflection at the surface); and (ii) a contribution from the phase β accumulated during propagation through the normal region, $\beta = 2L(k^e - k^h) + \beta_0$, where the first term corresponds to the ballistic motion and the second to the reflection at the NI interface. The electron/hole wavevectors are $\hbar k^{e,h} = [2m(E_F \cos^2\theta \pm E)]^{1/2}$. The Bohr–Sommerfeld quantization condition can then be written as

$$-(\gamma + \bar{\gamma}) \mp \delta\chi + \beta(E) = 2n\pi \tag{1}$$

where $\delta\chi = \chi - \bar{\chi}$, and where $\mp\delta\chi$ corresponds to quasiparticle trajectories in the $\pm k_y$ directions.

In the case of a uniform and isotropic order parameter ($\gamma = \bar{\gamma}$; $\chi = \bar{\chi}$), equation (1) reduces to

$$-2\gamma + \beta = 2n\pi \tag{2}$$

and leads to the spectral equation

$$E = \pm\Delta \cos\frac{\beta(E)}{2}. \tag{3}$$

According to this equation, surface states always exist, even at a simple IS interface ($L = 0$) due to the normal reflection phase shift $\beta_0 \neq 0$ in the superconducting electrode (Wendin and Shumeiko 1996a). However, in the presence of an INS well, $L \neq 0$, the ballistic contribution to β, $2L(k^e - k^h) \approx 4LE/\hbar v_F \cos\theta$, usually dominates, and the dispersion equation (3) takes the form found by de Gennes and Saint-James (1963),

$$\frac{E}{\Delta} = \pm\cos\frac{E}{\Delta}\frac{2L}{\xi_0\cos\theta}. \tag{4}$$

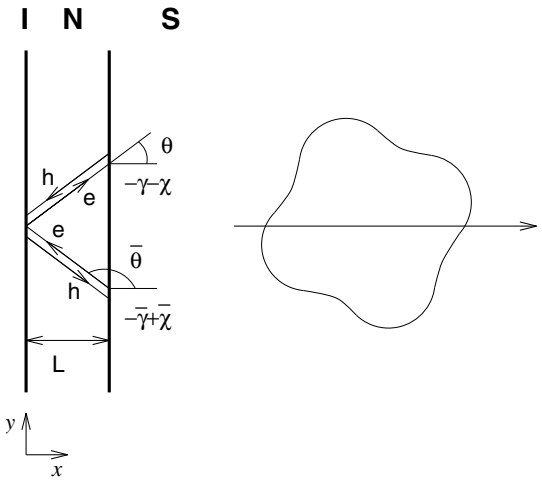

Figure 1. Quasiclassical path giving the bound states at a specular surface of a superconductor with anisotropic s-wave order parameter $\Delta(\theta)$ (schematically drawn in the right part of the figure). N is a normal region of size $L \sim \xi_0$ to model the gap suppression near the surface. The quasiparticles are trapped in the surface region because of normal reflection at the vacuum/metal (IN) surface and subgap Andreev reflection at the NS surface. The angle θ gives the propagation direction relative to the surface normal. During Andreev reflection, an electron (e) is converted into a hole (h) with the phase gain $-\gamma - \chi$. According to the Bohr–Sommerfeld quantization condition, the total phase accumulated during one cycle is equal to $2\pi n$.

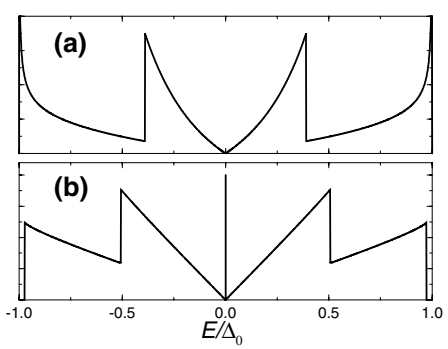

Figure 2. (a) Density of surface states at an s-wave superconductor surface with a normal metal overlayer of thickness $1.5\xi_0$. The peak energies are the bound states for trajectory angle $\theta = 0$ and the tails towards lower energies are due to the angle integration; for increasing angles θ the energy of the surface states are continuously shifted down relative to the $\theta = 0$ state. (b) The same for a gap of d-wave symmetry. The crystal is rotated by 45° relative to the surface normal so that MGS are formed (the delta peak at zero energy).

Generally, the electron–hole dephasing factor $\beta(E)$ is an odd function of the energy and turns to zero at $E = 0$. This is a result of the fact that the difference between electrons and holes vanishes at the Fermi surface. Due to this property there is no $E = 0$ solution of equation (3), and the density of surface states in s-wave superconductors is zero at the Fermi level; see figure 2(a). Moreover, due to the presence of time reversal symmetry in the problem, the surface levels always appear in pairs symmetrically positioned around the Fermi level.

The number of surface states for each quasiparticle trajectory is determined by the length of the quasiparticle path, which is given by the normal layer thickness and the propagation angle θ: for $L < \pi\xi_0$, equation (4) implies that for normal incidence ($\theta = 0$) there is a single pair of surface states close to the energy gap edge. A new pair of surface states appear at the gap edge when $1/\cos\theta = \pi\xi_0/L$. Increasing the trajectory angle further pushes these states down into the gap, and a new pair of gap edge states appears every time $1/\cos\theta$ is increased by $\pi\xi_0/L$. Integration over the angle θ yields the surface density of states plotted in figure 2(a); cf de Gennes and Saint-James (1963).

In anisotropic s-wave superconductors, different gap values before ($|\Delta|$) and after ($|\bar{\Delta}|$) normal reflection at the surface ($\gamma \neq \bar{\gamma}$) will modify the phase shifts of the Andreev reflections and change the energy of the surface state. Therefore, the surface states depend on how the surface is oriented relative to the crystal axes. The angle integration will then to a large extent wash out the peaks in the density of states (DOS) found in figure 2(a). Roughness of the interface will lead to further suppression of the peaks in the DOS and to the opening of a gap in the spectrum (Melsen *et al* 1996). In this review, however, we will not discuss rough interfaces in any detail. It is also worth mentioning that for anisotropic superconductors, the total DOS within the energy interval $\Delta_{min} < E < \Delta_{max}$, contains, in addition to the bound surface states, contributions from the continuum states.

The surface states are two-fold degenerate, the two states corresponding to different signs of the electron momentum ($\pm k_y$) parallel to the surface. In the presence of a magnetic field parallel to the surface, this degeneracy is removed due to the Meissner current: the spectrum calculated above holds in the frame of reference of the condensate. In the laboratory reference frame the levels are shifted by the Doppler term $p_s v_F \sin\theta$, $E \rightarrow E + p_s v_F \sin\theta$, where p_s is the superfluid momentum of the Meissner current. This shift has opposite signs for electrons moving along and against the Meissner current.

2.3. d-wave surface states

In the d-wave superconductors, the order parameter is angle dependent,

$$\Delta(\theta) = \Delta_0 \cos[2(\theta - \alpha)] \tag{5}$$

where α describes the orientation of the order parameter relative to the surface normal; see figure 3. Consequently, the gap (order parameter) is different before (Δ) and after ($\bar{\Delta}$) normal reflection. As long as Δ and $\bar{\Delta}$ have the same sign, i.e. the same phase, $\chi = \bar{\chi}$, the situation is not qualitatively different from the anisotropic s-wave case. However, the situation dramatically changes if Δ and $\bar{\Delta}$ have opposite signs, as illustrated in figure 3: in this case, the phases χ and $\bar{\chi} = \chi + \pi$ of these order parameters differ by $\delta\chi = \chi - \bar{\chi} = -\pi$, which leads to a modification of equation (2),

$$-(\gamma + \bar{\gamma}) + \pi + \beta(E) = 2n\pi. \tag{6}$$

This equation always has the root $E = 0$ since $\gamma(E = 0) = \bar{\gamma}(E = 0) = \pi/2$ and $\beta(E = 0) = 0$. This means that for the corresponding angle of incidence, a surface state will appear at zero-energy: this is the so-called MGS (Hu 1994). Clearly, this MGS is degenerate with respect to $\pm k_y$. It is

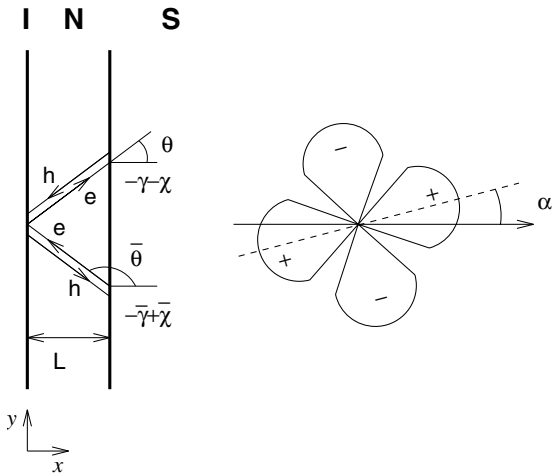

Figure 3. Quasiclassical path giving the bound states at a specular surface of a two-dimensional d-wave superconductor with order parameter $\Delta(\theta) = \Delta_0 \cos[2(\theta - \alpha)]$, where θ is the propagation angle (compare figure 1) and α is the orientation angle of the order parameter relative to the surface normal. N is a normal region of size $L \sim \xi_0$ to model the gap suppression near the surface.

easy to see that for the $\alpha = \pm\pi/4$ orientations, a MGS exists for every quasiparticle trajectory, $-\pi/2 < \theta < \pi/2$, while for the $\alpha = 0, \pi/2$ orientations there are no MGS at all. For arbitrary α, MGS exist within the window $\pi/2 - \alpha < |\theta| < \pi/2 + \alpha$. The formation of MGS is a robust property of d-wave superconductors: it requires only different signs of Δ and $\bar{\Delta}$ and does not depend on the possible difference in their absolute values. Moreover, the formation of a MGS is not sensitive to the spatial variation of $\Delta(x)$ (see appendix A4). This insensitivity is an important property, because in d-wave superconductors the gap is suppressed by the surface for most orientations of the crystallographic axes.

There is work in the literature addressing the questions of how surface roughness (Golubov and Kupriyanov 1999), impurities (Poenicke *et al* 1999), and nanofaceting of the surfaces/interfaces (Fogelström *et al* 1997) affect the MGS. However, in this review we will focus on clean ballistic structures with specularly reflecting interfaces, and we refer the reader to the original literature (e.g. the abovementioned papers and references therein).

The major effect of taking gap suppression into account will be the presence of additional bound states in the vicinity of the gap edge. Fully self-consistent calculations have been performed by, for example, Nagato and Nagai (1995), Buchholtz *et al* (1995a, b), Matsumoto and Shiba (1995a,b, 1996) and Barash *et al* (1997). Qualitatively, the effect of the surface levels at finite energy can be understood by considering a rectangular SNI well of size $L \sim \xi_0$. For the sake of illustration, let us consider the $\alpha = \pi/4$ orientation for which a MGS exists for every trajectory angle θ (see figure 3). We then have $|\Delta| = |\bar{\Delta}|$, and equation (6) reduces to

$$\frac{E}{|\Delta|} = \pm \sin \frac{E}{|\Delta|} \frac{2L}{\xi_0 \cos\theta}. \tag{7}$$

The resulting density of bound states for a normal metal length $L = 1.5\xi_0$ is shown in figure 2(b). Note that the density of surface states in this figure is only the part of the DOS with $|E| < \Delta_{max}$, similar to the anisotropic s-wave case; there is also a considerable contribution from the extended states of the bulk due to the gap nodes.

2.4. Impurity induced MGS

The above discussion was focused on MGS at planar surfaces. However, it is clear that MGS must exist at any defect which produces quasiparticle scattering between states θ and $\bar{\theta}$ corresponding to different signs of the order parameter: cracks, twin boundaries, impurities, etc. Thus, a direct measurement of the DOS at zero energy by scanning tunnelling microscopy (STM) in the vicinity of an impurity can test the d-wave symmetry of the order parameter. Such experiments were recently performed by Yazdani *et al* (1999), Hudson *et al* (1999) and Pan *et al* (2000a). We shall discuss these experiments later, at the end of section 4, which is devoted to a discussion of current transport through MGS.

2.5. Paramagnetic effect of MGS

Another possibility to detect the impurity induced MGS was demonstrated in the experiment by Walter *et al* (1998) (figure 4) and recently by Carrington *et al* (2001), where the response to an external magnetic field was studied. In this experiment, the MGS were introduced in a *c*-oriented $YBa_2Cu_3O_x$ (YBCO) film by creating multiple quasi-1D in-plane defects (ion tracks) by ion bombardment. By varying the orientation of the ion beam, and therefore the ion tracks, with respect to the order parameter, it was possible to control the density of MGS. In the experiment, the temperature dependence of the magnetic penetration depth $\lambda(T)$ was measured for different orientations of the defects (figure 4). It was found that for (110) orientation $\lambda(T)$ has a minimum below 15 K and increased with decreasing temperature, while for (100) orientation the low-temperature upturn was much smaller.

This effect can be explained within the above picture by studying the paramagnetic response of MGS to an applied magnetic field (Higashitani 1997). As was mentioned in section 2.2, the surface states undergo splitting in the presence of a magnetic field. The energy of an individual MGS becomes $E_{MGS}(\theta) = p_F v_{sy} \sin\theta$, where v_{sy} is the superfluid velocity along the surface of the defect. Since the MGS are localized over a distance much smaller than the penetration depth ($\xi_0 \ll \lambda$), the non-homogeneity of the superflow can be neglected. The MGS current per *ab*-plane along the surface is $j_{MGS} = ev_F \sin\theta |\psi_{MGS}(x)|^2 n_F[E_{MGS}(\theta)]$. The total current of all MGS at the defect is calculated by integrating over x and also over k_y, $-k_F < k_y < k_F$. At zero temperature, $T = 0$, only the negative energy levels ($k_y < 0$), which carry paramagnetic current, are occupied, which leads to a total current $j_{MGS} = -eE_F/2\pi\hbar$ at the defect (for (110) orientation). By dividing this equation by d, the average distance between the defects, we get the average density of the paramagnetic MGS current. At finite temperature, the positive energy levels carrying diamagnetic current also become occupied, which leads to a reduction of the paramagnetic effect. When $T \gg p_F v_s$, expansion of the Fermi function and integration over k_y yield a $1/T$ dependence for the average MGS current density,

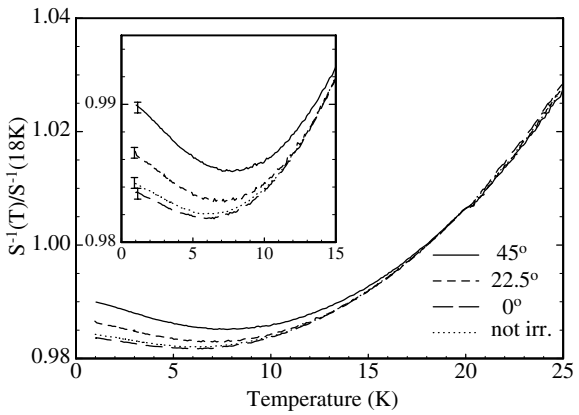

Figure 4. Temperature dependence of the penetration depth $\lambda(\propto S^{-1})$ measured on YBCO films containing differently oriented linear defects introduced via ion bombardment. Due to the presence of MGS at the defects, which respond paramagnetically to an external field, there is an upturn of λ at low temperature. The upturn in the unirradiated film is thought to be due to MGS at internal interfaces (grain boundaries). What is important is the enhancement of the paramagnetic effect with increasing orientation angle (compare the angle α in figure 3) from 0 to 45° of the defects, (from Walter *et al* (1998)).

$j_{MGS} = -(eE_F/6\pi\hbar d)(p_F v_s/T)$. This paramagnetic current is to be added to the paramagnetic current of the quasiparticles in the bulk of the d-wave superconductor, $j_n = -ev_s n_n(T)$, where $n_n(T)$ is the density of quasiparticles which linearly depends on the temperature, $n_n(T) \sim (k_B T/\Delta)n$, at $k_B T \ll \Delta$ (n is the electron density).

This interplay of the bulk quasiparticle current and the MGS current produces the low-temperature anomaly of the magnetic penetration depth observed in the experiment (Walter *et al* 1998). The effect is most pronounced for (110) orientation, and disappears for (100) orientation of the defects because of the absence of MGS in the latter case. In the experiment, the effect did actually not disappear for the (100) orientation, but was a minimum. The finite value was explained to be due to MGS at internal interfaces in the film, for example grain boundaries.

2.6. Splitting of MGS

Although the d-wave symmetry of the gap necessarily leads to the formation of MGS, the resulting large density of states at the Fermi level is actually energetically unfavourable: any mechanism able to split the MGS and produce a gap in the spectrum will lower the energy of the system (Sigrist 1998, Fogelström and Yip 1998). Different mechanisms splitting the MGS have been proposed in the literature: (1) splitting due to a subdominant component of the order parameter which forms a local complex $d \pm is$ gap parameter at the surface, (2) self-induced Doppler shifts, and (3) formation of a spin-density wave near the surface. Here, we shall discuss the first two mechanisms in greater detail, while for the third scenario, we refer to the original literature (Honerkamp and Sigrist 1999; Honerkamp *et al* 2000).

2.6.1. $d \pm is$ order parameter. For orientations where the d-wave gap is suppressed and at low temperatures, a subdominant gap of s or d_{xy} symmetry may appear near the surface if a weak secondary interaction (additional to the one responsible for the d-wave superconductivity) is present (Matsumoto and Shiba 1995a, b, 1996; Fogelström *et al* 1997, Tanuma *et al* 1999, Zhu *et al* 1999). In a self-consistent picture, the complex combination $\Delta_{d_{x^2-y^2}} \pm i\Delta_s$ (or $\Delta_{d_{x^2-y^2}} \pm i\Delta_{d_{xy}}$) is energetically favourable. The MGS is sensitive to the presence of this subdominant gap; to demonstrate this, let us consider the order parameter $\Delta_{d_{x^2-y^2}} + i\Delta_s$ with the d-wave component having $\alpha = \pi/4$ orientation. We now define a relative phase angle $\chi_{rel} = \arctan(\Delta_s/\Delta_d)$. In this case, the scattering phase shift during Andreev reflection has the additional contribution $+\chi_{rel}$ for $k_y > 0$, and $-\chi_{rel}$ for $k_y < 0$. In a symmetric case with $\gamma = \bar{\gamma}$, we get the following modification of equation (6) at low energies:

$$-2\gamma \mp 2\chi_{rel} + \pi = 2n\pi. \tag{8}$$

The effect of this $\pm k_y$-dependent contribution from the relative phase is to shift the MGS away from the Fermi level to the edges of the subdominant gap,

$$E_{MGS} = -(\operatorname{sgn} k_y)\Delta_s \tag{9}$$

and the $\pm k_y$ degeneracy of the MGS is lifted. This splitting of the MGS is a result of the broken time-reversal symmetry in the $\Delta_d + i\Delta_s$ state. The MGS splitting drives the instability (lowers the energy of the system) which appears at a critical temperature determined by the strength of the subdominant interaction. Each bound state carries current parallel to the surface in the direction given by k_y, which means that at low temperatures, when only the state below the Fermi energy is occupied (the one labelled $+k_y$ for $\Delta_s > 0$ in equation (9)), a net surface current will be present. This spontaneous current manifests the broken time-reversal symmetry of the order parameter (Sigrist 1998). The time-reversal symmetry breaking (TRSB) state is two-fold degenerate: the gap parameter can be either $d + is$ or $d - is$, corresponding to the two possible directions of the spontaneous surface current.

The spectrum of surface states in $d + is$ superconductors has a close similarity to the spectrum in a B-phase p-wave superconductor. In the light of the above discussion, it is therefore straightforward to understand the results obtained by Buchholtz and Zwicknagl (1981). The B-phase gap parameter in a two-dimensional p-wave superconductor can be written $\Delta_{\sigma\sigma} = \Delta(\sigma\cos\theta + i\sin\theta)$ ($\sigma = \pm 1$ for down/up spins), see e.g. the book by Vollhardt and Wölfle (1990). This gap function is similar to the $d + is$ case above, but with a propagation-angle-dependent magnitude of the imaginary component $i\Delta\sin\theta$. Thus, there are surface bound states also for p-wave superconductors; however, the bound state is located at the Fermi level only for quasiparticles propagating perpendicular to the surface ($\theta = 0$), since the gap is real (and changes sign at the normal reflection event) only for this particular propagation angle. Integrating over the injection angle, we find that the density of states is finite for all subgap energies, and there is no zero energy peak (Buchholtz and Zwicknagl 1981). We conclude that the density of bound surface states of p-wave and d-wave superconductors are quite different, although the mechanism of the bound state formation is the same.

2.6.2. Doppler shifts. In connection with the discussion of the paramagnetic effect, Higashitani (1997) discovered that the MGS are unstable, even in the absence of any subdominant interaction (pure d-wave order parameter), due to the possibility of creation of spontaneous magnetic fields. As we discussed in the previous section, a splitting of MGS yields a surface current at low temperature. This current creates a magnetic field which is screened by a supercurrent counterflow which, in turn, further splits the MGS due to the Doppler shift effect discussed in section 2.2. The effect saturates when the magnetic energy compensates for the energy of the Doppler shifted MGS. Thus, a TRSB state spontaneously occurs, with a surface current due to the split MGS and a self-consistent screening current upholding the Doppler shifts at a phase transition temperature $k_B T_{TRSB}/\Delta_0 = (1/6)(\xi_0/\lambda)$ (Honerkamp and Sigrist 1999, Barash *et al* 2000, Löfwander *et al* 2000) which is much smaller than the critical temperature of the type II superconductors ($\xi_0 \ll \lambda$).

3. Dc Josephson effect

In this section we shall discuss how, from a theoretical point of view, MGS influence the dc Josephson effect. First, we develop the concept of Andreev bound states and explain how they in many cases determine the properties of Josephson junctions. Then we discuss some particular junction orientations which illustrate some effects peculiar for Josephson junctions of d-wave superconductors: large Josephson currents proportional to $\sqrt{D}$ (D is the junction transparency), $1/T$ dependence (T is the temperature) of the Josephson critical current, π-junction formation, $0 \to \pi$ junction crossovers with temperature, and spontaneous TRSB.

3.1. Andreev states: coupled surface states

When two superconducting electrodes are connected to form a junction, the superconducting surface states form coherent bound states of the entire junction, Andreev bound states. There is an obvious analogy with a double well system. The structure of the Andreev state is illustrated in figure 5. Like the surface states, the Andreev state consists of a combination of electron and hole wavefunctions with opposite electron momenta k_x (momentum k_y parallel to the specular surface is conserved). The analogy with the double well system allows us to expect that the Andreev levels will be split and shifted with respect to the surface levels, the shift depending (i) on the transparency of the tunnel barrier separating the electrodes and (ii) on the superconducting phase difference across the junction. Taking into account the phase dispersion of the energy ($\mathrm{d}E/\mathrm{d}\phi$) of the Andreev levels, one may talk about Andreev bands $E(\phi)$ with width (dispersion) proportional to the junction transparency D. However, if the surface states at the two sides of the junction have equal energies, the coupling becomes resonant. In this *resonant* case, the splitting of the levels, and therefore the width of the Andreev band, will be particularly large and proportional to $\sqrt{D}$ (Wendin and Shumeiko 1996a). As we will see, the width of the Andreev band determines the critical Josephson current, and the Andreev band dispersion determines the Josephson current–phase relation. One might expect the surface states to be degenerate in junctions fabricated with the same superconducting material; however, even in this case the degeneracy can be lifted due to several types of asymmetries, e.g. misorientation of the order parameters, difference in spatial modulation of the the order parameters, etc.

The derivation of the spectral equation for the Andreev states is more involved than the derivation of the spectrum of surface states. The properties of the Andreev levels can therefore not be strictly deduced from simple quasiclassical arguments but rather require solving of the Bogoliubov–de Gennes (BdG) equation (de Gennes 1989). However, the spectral equation can be presented in terms of the earlier introduced phase shifts γ_L (γ_R) and β_L (β_R) in the left (L) and right (R) electrodes of the junction, and the superconducting phase difference $\phi = \chi_L - \chi_R$. We here choose to define the Andreev reflection phase γ for negative Δ as $\gamma = \arccos(E/|\Delta|) + \pi$. The spectral equation then becomes

$$\cos a = R(\theta)\cos b + D(\theta)\cos c \tag{10}$$

where

$$2a = -\gamma_L - \bar{\gamma}_L - \gamma_R - \bar{\gamma}_R + \beta_L + \beta_R$$

$$2b = -\gamma_L - \bar{\gamma}_L + \gamma_R + \bar{\gamma}_R + \beta_L - \beta_R$$

$$2c = -\gamma_L + \bar{\gamma}_L - \gamma_R + \bar{\gamma}_R - 2\phi.$$

Equation (10) describes hybridization of the surface states. This is obvious if one lets the transparency $D(\theta) \to 0$, in which case one recovers equation (6) for decoupled surface states. However, equation (10) can also be interpreted as hybridization of Andreev states present in the corresponding perfectly transparent junction ($D = 1$) due to normal electron back scattering at the insulating barrier. The spectral equation for Andreev states in perfectly transparent junctions actually follows from quasiclassical arguments:

$$-\gamma_L - \gamma_R + \beta_L + \beta_R - \phi = 2n\pi$$

$$-\bar{\gamma}_L - \bar{\gamma}_R + \bar{\beta}_L + \bar{\beta}_R - \phi = 2n\pi \tag{11}$$

where the first and second lines correspond to the decoupled θ and $\bar{\theta}$ segments in figure 5.

3.2. Josephson current

Since Andreev reflection is accompanied by charge transfer through the NIS interface, the Andreev states are able to carry current. The current through the surface states is blocked in the direction perpendicular to the surface due to complete quasiparticle reflection from the insulator. In the NIS junction, this insulating interface becomes transmissive, and the current may flow through the Andreev states. There is a general relation between the current through the Andreev state and the phase dispersion of the energy of the Andreev state,

$$I_x = \frac{2e}{\hbar}\frac{\mathrm{d}E}{\mathrm{d}\phi}. \tag{12}$$

This equation can be derived directly from the BdG equation (Shumeiko *et al* 1997) or deduced from the thermodynamical equation $I = (2e/\hbar)\partial F/\partial\phi$ by using a microscopic expression for the junction free energy (Beenakker 1991). The total

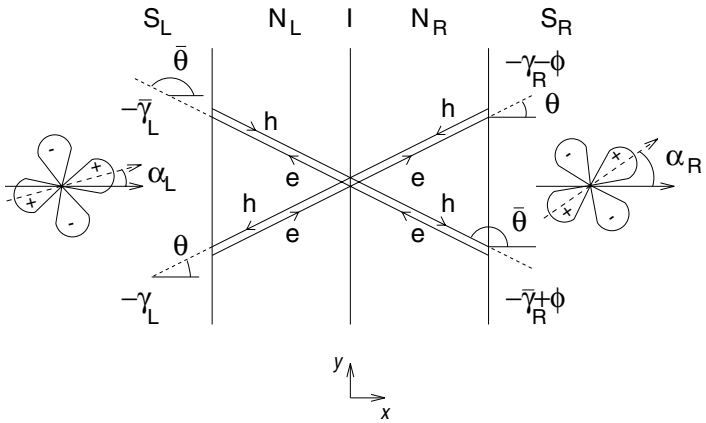

Figure 5. Quasiclassical trajectory illustrating the Andreev bound state in a specular two-dimensional superconductor junction. S_L and S_R are the left and right d-wave superconductor electrodes with orientation angles α_L and α_R, respectively. The junction region consists of a barrier (insulator I) and normal regions N_L and N_R which may be due to the gap suppressions. The Andreev state can be thought of as a hybridization of the surface states (figure 3) of the left and right sides of the insulator.

Josephson current of the bound states per unit surface area, per *ab*-plane, flowing perpendicular to the surface is

$$j_x = \frac{2ek_F}{h} \sum_n \left\langle \frac{\mathrm{d}E_n}{\mathrm{d}\phi} n_F(E_n) \right\rangle \tag{13}$$

where the angle brackets denote integration over the trajectory angle θ,

$$\langle \cdots \rangle = \int_{-\pi/2}^{\pi/2} \mathrm{d}\theta \cos\theta. \tag{14}$$

The Josephson current in d-wave junctions strongly depends on the orientation of the order parameters in the electrodes with respect to the junction interface. The whole picture is quite complex, however one can distinguish three qualitatively different cases: (i) no MGS at any side of the junction, (ii) MGS at both sides of the junction, and (iii) a MGS at one side of the junction. For arbitrary orientation all three cases may occur for different sectors of the trajectory angle θ, and the total current is a weighted sum of currents of the three types. In a pure form, the first case is realized in $\mathrm{d}_0/\mathrm{d}_0$ junctions where the situation is similar to s-wave junctions: no suppression of the order parameter, and the two Andreev bound states which dominate the Josephson current are situated close to the gap edges and have dispersion of order D. The second case is realized in a pure form in $\mathrm{d}_{\pi/4}/\mathrm{d}_{\pm\pi/4}$ junctions. In this case, the central phenomenon is the *resonant coupling of MGS*, which produces large current proportional to $\sqrt{D}$ with rather special properties. We choose to illustrate the third case by the $\mathrm{d}_0/\mathrm{d}_{\pi/4}$ junction. The peculiarity of this case is the TRSB.

In many works, for example Sigrist and Rice (1995), it has been assumed that tunnelling occurs only for normal incidence, $\theta = 0$. This is motivated by the discriminating effect of the *tunnelling cone* (Wolf 1985). However, in order to include the effects of MGS it is very important to actually take a wide tunnelling cone $D(\theta)$ into account, since tunnelling through MGS only occurs at finite angles of incidence. Ignoring this point, one might conclude that the Josephson current is zero, or at least small, for the $\mathrm{d}_{\pi/4}/\mathrm{d}_{\pi/4}$ orientation since $\Delta(\theta = 0) = 0$. However, this will be true only for a cone very strongly peaked around $\theta = 0$, since the MGS contribution for the finite cone angle is resonant. Clearly, the exact functional dependence of the current on orientation will be sensitive to the actual shape of the cone and not only to the value of the junction transparency $\langle D \rangle$. Throughout this review we use a δ-function model for the barrier. In this case the cone is quite wide, $D(\theta) \sim \cos^2\theta$ (see, for example, Bruder (1990)), and the effects of MGS are somewhat overemphasized. An exception is the treatment of the $\mathrm{d}_0/\mathrm{d}_{\pi/4}$ orientation below, where we instead follow Löfwander *et al* (2000) and use a wide barrier model which has $D(\theta) \sim \exp(-\kappa\theta^2)$, where κ determines the width of the cone and is a function of the barrier height and width (Wolf 1985). However, even in this case the MGS contribution will dominate at low temperature, as discussed below.

3.2.1. $d_{\pi/4}/d_{\pi/4}$ orientation: 0-junction with large I_c. The order parameter for this orientation is strongly suppressed by the surface; however, the qualitative properties of MGS in junctions with low transparency $D \ll 1$ are not sensitive to the detailed profile of the order parameter, which allows us to consider the rectangular well model.

For this high-symmetry orientation, the four gaps in equation (10) have equal magnitudes, $|\Delta_L| = |\bar{\Delta}_L| = |\Delta_R| = |\bar{\Delta}_R|$. The π shift at both sides is picked up at $\bar{\theta}$ (Andreev reflecting against a negative lobe of the order parameter). The spectral equation takes the form

$$\cos(2\gamma - \beta) = -R(\theta) + D(\theta)\cos(\phi) \tag{15}$$

which, for small energies $E \ll \Delta$ and negligible dephasing ($\beta = 0$), has the solution (Riedel and Bagwell 1998)

$$E_\pm = \pm|\Delta|\sqrt{D}\cos\frac{\phi}{2} \tag{16}$$

plotted in figure 6(a). The current of these two MGS is calculated via equation (13). At zero temperature, only the level below zero energy is populated while the level above is empty, and the current is

$$j_{MGS} = \frac{ek_F}{h}\langle|\Delta|\sqrt{D}\rangle \sin\frac{\phi}{2}\,\mathrm{sgn}\left(\cos\frac{\phi}{2}\right). \tag{17}$$

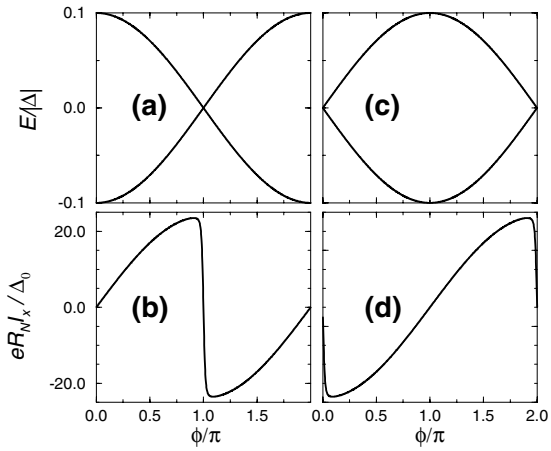

Figure 6. (a) Dispersion relation $E(\phi) = \Delta(\theta)\sqrt{D(\theta)}\cos\phi$ for the Andreev bound states in the specular d-wave junction with orientation $d_{\pi/4}/d_{\pi/4}$ for the injection angle $\theta = \pi/4$. The transparency is $D(\theta = \pi/4) = 0.01$. (b) Angle integrated current–phase relation for the same junction for very low temperature ($T = 0.003T_c$). (c), (d) The same but for the orientation $d_{\pi/4}/d_{-\pi/4}$. In this case the dispersion relation is $E(\phi) = \Delta(\theta)\sqrt{D(\theta)}\sin\phi$ and the current is π-shifted relative to the $d_{\pi/4}/d_{\pi/4}$ case. The angle averaged transparency is $\langle D\rangle = 0.026$.

The critical (maximum) Josephson current is proportional to $\sqrt{D}$ (Tanaka and Kashiwaya 1996a, Riedel and Bagwell 1998 and Barash 2000) and is much larger than the Ambegaokar–Baratoff critical current in non-resonant s-wave tunnel junctions, which is proportional to D (Anbegokar and Baratoff 1963). In figure 6(b), we plot the current–phase relation at low temperature. Note that the $\sqrt{D}$ behaviour is a general phenomenon connected with resonance coupling (Wendin and Shumeiko 1996a).

To understand the basic temperature dependence of the current, we notice that the two MGS energies $E_\pm$ carry currents in opposite directions, $j_+ = -j_-$, and therefore with increasing population of the upper level at large temperature, the current carried by MGS will decrease,

$$j_{MGS} = \frac{2ek_F}{h}\left\langle \frac{dE_+}{d\phi} n_F(E_+) + \frac{dE_-}{d\phi} n_F(E_-)\right\rangle = -\frac{2ek_F}{h}\left\langle \frac{dE_+}{d\phi}\tanh\frac{E_+}{2k_BT}\right\rangle. \quad (18)$$

The scale of the temperature dependence of the current is set by the well defined energy difference of the two-level MGS system. When $E_+ \ll k_BT$, the expansion $\tanh x \approx x$ leads to a $1/T$ dependence of the current (Tanaka and Kashiwaya 1996a, Barash *et al* 1996, Riedel and Bagwell 1998),

$$j_{MGS} = \frac{2ek_F}{h}\frac{\sin\phi}{8k_BT}\langle D|\Delta|^2\rangle. \quad (19)$$

In tunnel junctions, the current carried by MGS dominates at low temperature $k_BT \leqslant E_+$ because the continuum state current is proportional to the junction transparency D. Due to suppression of the gap at the interface, there are also Andreev states near the gap edges which may carry large currents due to degeneracy of the corresponding surface states. However, the net current of these states is also of order D since they

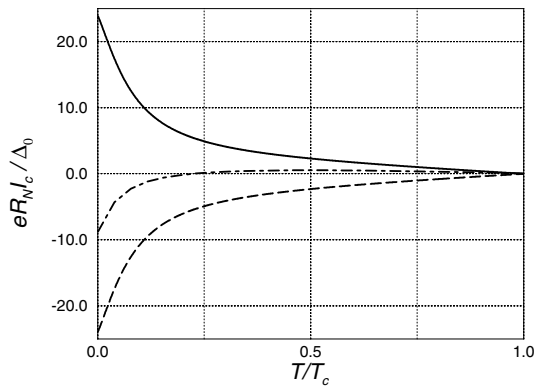

Figure 7. Critical current as a function of temperature for three different orientations of the d-wave superconductors: $d_{\pi/4}/d_{\pi/4}$ (full curve), $d_{\pi/4}/d_{-\pi/4}$ (dashed curve), and $d_{\pi/8}/d_{-\pi/8}$ (dot–dashed curve). The negative sign of I_c indicates that the junction minimum is at $\phi = \pi$ (π-junction). The $0 \to \pi$ junction crossover with decreasing temperature for the $d_{\pi/8}/d_{-\pi/8}$ junction is due to the competition between the MGS currents (dominating at low temperature) and current contributions from gap–edge bound states and continuum states (dominating at high temperature). The angle averaged junction transparency is $\langle D\rangle = 0.026$.

form pairs far below the Fermi level that are almost equally populated. The currents carried by the two bound states of the pair flow in opposite directions and cancel each other. Thus we conclude that the critical current I_c scales with temperature as $1/T$ for low temperatures, as clearly seen in figure 7 (the full curve). In the limit $T \to 0$, the $I_c(T) \propto 1/T$ dependence approaches a maximum value $I_c(0) \propto |\Delta|\sqrt{D}$, see equation (17).

3.2.2. $d_{\pi/4}/d_{-\pi/4}$ orientation: π-junction with large I_c. From a technical point of view, this case is very similar to the previous one, the difference being that the π shift at the right side is now picked up at θ rather than at $\bar\theta$ (because the positive and negative lobes of the order parameter have changed places). This results in a phase shift $\phi \to \phi + \pi$ in equation (15) which now reads

$$\cos(2\gamma - \beta) = -R(\theta) - D(\theta)\cos(\phi) \quad (20)$$

with the MGS solution (Riedel and Bagwell 1998)

$$E_\pm = \pm|\Delta|\sqrt{D}\sin\frac{\phi}{2}. \quad (21)$$

The MGS band again has a large dispersion proportional to $\Delta\sqrt{D}$; however, the phase dependence is π shifted compared to the $d_{\pi/4}/d_{\pi/4}$ junctions (see figure 6(c)). The current–phase relation will therefore also be π-shifted (see figure 6(d)) which puts the minimum of the junction energy at a phase difference equal to π instead of 0, corresponding to a π-junction. This fact was used in the tri-crystal ring experiments, although the theoretical idea behind the experiment put forward by Geshkenbein *et al* (1987) and later on by Sigrist and Rice (1995) was based on symmetry arguments and not on the microscopic picture outlined here.

Again, the critical current has the low-temperature anomaly, $I_c(T) \propto 1/T$ and approaches a maximum value $I_c(0) \propto |\Delta|\sqrt{D}$ at zero temperature (dashed curve in figure 7). To emphasize the π-junction behaviour, we let the critical current be negative in this case.

3.2.3. $d_\alpha/d_{-\alpha}$ orientation: 0- to π-junction cross-over. We are now able to discuss general properties of the Josephson current in symmetric junctions $d_\alpha/d_{-\alpha}$; see Barash *et al* (1996), Tanaka and Kashiwaya (1996a, 1997, 1999) for a detailed discussion. In these junctions, MGS exist only within certain limited intervals of the angle θ while for other angles, the Andreev level spectrum is similar to the one in s-wave junctions and the corresponding currents follow the Ambegaokar–Baratoff law. At low temperature, the MGS will dominate and the equilibrium phase difference is, as in the $d_{\pi/4}/d_{-\pi/4}$ case, at $\phi = \pi$. However, at larger temperatures this contribution will be suppressed and the non-MGS current may dominate. This s-wave type current will give a minimum of the junction energy at $\phi = 0$. Hence, with an increase in the temperature, the junction will undergo a transition from a π-junction to an ordinary junction (Barash *et al* 1996, Tanaka and Kashiwaya 1996a). The critical current is zero at the transition temperature where there is detailed balance between the MGS current and the s-wave like current. We illustrate this behaviour with the $d_{\pi/8}/d_{-\pi/8}$ junction, the dot–dashed line in figure 7.

3.2.4. $d_{\pi/4}+is/d_{-\pi/4}+is$ Orientation: 0-junction re-entrance. Development of a subdominant s-wave order parameter near the junction interface leads to an interesting modification of the low-temperature anomaly of the critical current. As we discussed earlier, in the presence of a complex order parameter $\Delta_d + i\Delta_s$ the MGS are split into two states $E_{MGS} = \pm\Delta_s$, where the sign depends on the sign of the k_y wavevector. Thus the Andreev spectrum presented in figure 6 will move either up or down (for opposite signs of k_y) as soon as the subdominant gap Δ_s appears and grows with decreasing temperature. Let us consider the limit $\Delta_s(0) \gg |\Delta|\sqrt{D}$ where the effect is most pronounced. In this case, the Andreev bands do not cross the Fermi level at $T = 0$; the lower pair of levels is then fully occupied, while the upper pair is empty and therefore does not contribute to the current. This leads to an uncompensated y-current along the interface. Large x-currents carried by the occupied levels flow in opposite directions and cancel each other, leading to a small (for $D \ll 1$) residual current proportional to the first power of the junction transparency D. This residual current has a positive sign, similar to the common situation in s-wave SIS and SNS junctions (Wendin and Shumeiko 1996a, Samuelsson *et al* 2000), and therefore the π-junction property is lost. Thus the Josephson current undergoes a crossover from π-junction to 0-junction when the temperature decreases, and the critical current has a non-monotonic temperature dependence and turns to zero at the crossover point (Tanaka and Kashiwaya 1998), see figure 8. Experimental observation of such *reentrant* temperature dependence of the critical current would be direct evidence of the subdominant order parameter.

3.2.5. $d_0/d_{\pi/4}$ orientation: π-periodicity. For the $d_0/d_{\pi/4}$ orientation, there are MGS only at one side of the junction, corresponding to the non-resonant case. The spatial shapes of the order parameters are different at the two sides of the junction which also leads to non-resonant coupling of the non-MGS surface states. To understand the type of bound states present in this junction, we solve the spectral equation for the

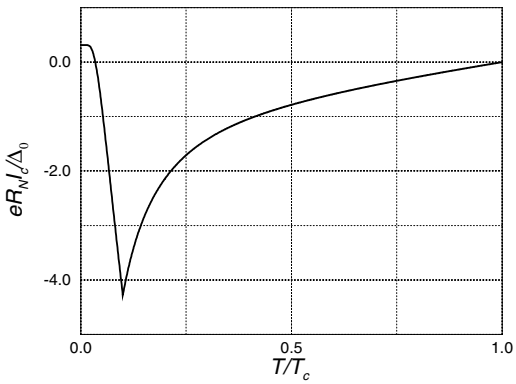

Figure 8. Critical current for the $d_{\pi/4}/d_{-\pi/4}$ orientation. At low temperature, T_s, a subdominant component of the order parameter with s-wave symmetry is assumed to appear and be $\pi/2$ out of phase with respect to the dominant d-wave component. This results in a cut-off of the MGS contribution and the junction changes from a π-junction to a 0-junction when the temperature is decreased.

injection angle $\theta = \pi/8$ when all four d-wave gaps involved have equal magnitudes $|\Delta(\pm\pi/8)| = \Delta_0/\sqrt{2}$. The spectral equation then takes the form [$D = D(\pi/8)$, $\Delta = \Delta(\pi/8)$]

$$\sin(2\gamma - \beta) = \pm D \sin(\phi) \tag{22}$$

where the different signs correspond to quasiparticle states with $\mp k_y$. The solution for $\beta = 0$ is given by

$$E^2 = \frac{\Delta^2}{2}(1 \pm \sqrt{1 - D^2 \sin^2 \phi}). \tag{23}$$

There are two Andreev bands for a given k_y, the MGS band and the band at the gap edge (Riedel and Bagwell 1998). The dispersion of the MGS band is proportional to D at low transparency,

$$E_{MGS} = -\operatorname{sgn} k_y \frac{\Delta}{2} D \sin\phi + \mathrm{O}(D^2) \tag{24}$$

while the dispersion of the Andreev band at the gap edge is much smaller, proportional to D^2. Equation (24) is a good approximation for all injection angles in the low transparency limit when the MGS are well inside the gap, close to zero.

For the orientations discussed in the previous sections, the MGS spectrum is degenerate with respect to $\pm k_y$: in other words, there is a pair of MGS, $E_\pm$, for every k_y. In the present case, however, this degeneracy is lifted as emphasized in figure 9(a). Inspection of the MGS wavefunctions for phase differences between zero and π shows that, at a large distance from the interface, the E_- wavefunction decays only for $+k_y$, while for $-k_y$ it grows exponentially. For the E_+ wavefunction the situation is the opposite: the wavefunction decays for $-k_y$ and grows exponentially for $+k_y$. This difference between the two time-reversed states labelled by $\pm k_y$ is a consequence of the sign difference between the d-wave lobes and is the key point in understanding the possibility of spontaneous TRSB (see below).

The current in the $d_0/d_{\pi/4}$ junction is π-periodic, as opposed to the usual 2π-periodicity, as was first theoretically predicted in Yip *et al* (1990), Yip (1993), Tanaka and Kashiwaya (1997), Zagoskin (1997) and Östlund (1998), and

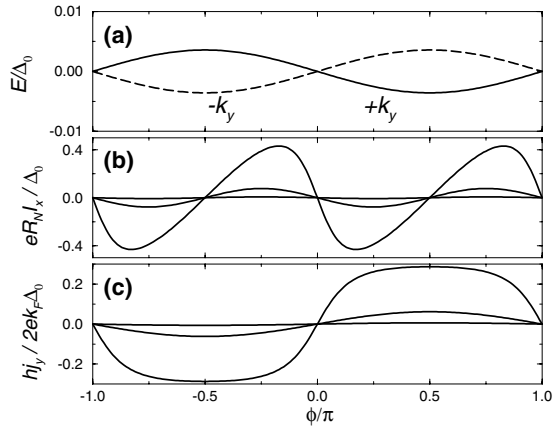

Figure 9. (a) Andreev bound states in a specular d-wave junction with the $d_0/d_{\pi/4}$ orientation for the injection angle $\theta = \pi/9$ and transparency $D(\theta = \pi/9) \approx 0.01$. The full and dashed curves are the $+k_y$ and $-k_y$ states, respectively. (b) The angle integrated current–phase relation for this orientation at three different temperatures: $T = \{0.001, 0.01, 0.1\}T_c$. (c) Phase dependence of the surface current density calculated to the right of the barrier for the same three temperatures. As the temperature is decreased, the $\pm k_y$ MGS become unequally populated and start to dominate the Josephson current which then is enhanced and is of order D. At the same time the surface current becomes appreciable.

later on measured in experiments by Ilichev *et al* (1999). At low temperatures the MGS band dominates the current–phase relation plotted in figure 9(b) and the bound states in equation (23) give $I_c(T) \propto D^2|\Delta|^2/k_BT$. However, at high temperatures, I_c will be negligibly small already for temperatures of the order $|\Delta|D$, in contrast to the $d_{\pi/4}/d_{\pi/4}$ case where this happens for temperatures of the order $|\Delta|\sqrt{D}$. This difference is a result of the larger energy scale given by the large dispersion of the bound states ($\propto \sqrt{D}$) in the resonant $d_{\pi/4}/d_{\pi/4}$ case compared to the much smaller dispersion ($\propto D$) in the non-resonant $d_0/d_{\pi/4}$ case.

3.2.6. $d_0/d_{\pi/4}$ orientation: TRSB. The current through the junction is zero for the phase differences $\phi = n\pi/2$. However, the minimum junction energy is achieved for $\phi_{eq} = \pm\pi/2$, since the MGS energy is the lowest for these phase differences. Due to the uneven occupation of MGS with opposite signs of k_y, the current parallel to the interface is finite even in equilibrium; see figure 9(c). For example, at $\phi_{eq} = \pi/2$, only MGS with positive k_y are occupied and a surface current is flowing in the positive y-direction. The opposite happens for $\phi_{eq} = -\pi/2$. Remembering that the state with $-k_y$ is obtained from the $+k_y$ state by the time-reversal operation, and noting that there is no way of taking the time-reversed state to the original state by adding an integer number of 2π to ϕ, we must conclude that time-reversal symmetry is spontaneously broken at the $d_0/d_{\pi/4}$ junction. This fact is manifested by the finite surface current, which produces a magnetic field at the junction.

The Josephson energy gain for $\phi_{eq} = \pm\pi/2$ is partly compensated by the energy cost of setting up the Meissner screening currents which ensure that the spontaneous magnetic field vanishes in the bulk superconductors far from the junction. By calculating the thermodynamic potential for the junction system (Löfwander *et al* 2000) it can be shown that the TRSB state really is favourable. If the orientation is not exactly $d_0/d_{\pi/4}$, the equilibrium phase difference ϕ_{eq} is shifted from $\pm\pi/2$. However, the TRSB effect (i.e. $\phi_{eq} \neq 0$ or π) remains for deviations up to about 10° (Yip 1997, Löfwander *et al* 2000) from the $d_0/d_{\pi/4}$ orientation.

Since there are screening currents flowing, we may expect Doppler shift effects. For transparencies $D \gg \xi_0/\lambda$, the dispersion of the MGS with phase difference, given by equation (24), is much larger than the Doppler shifts; these can therefore be neglected and the picture outlined above holds. However, for $D \ll \xi_0/\lambda$ the Doppler shifts dominate, and the problem is formally the same as MGS at a free surface, as discussed in section 2.6.

The above discussion of the $d_0/d_{\pi/4}$ junction, including the crossover to the Doppler shift driven TRSB surface instability, closely follows that presented in the paper by Löfwander *et al* (2000). The possibility of TRSB in purely d-wave junctions was first pointed out by Yip (1995) for the pin hole geometry, which is equivalent to having $D = 1$. Many people, using different theoretical tools, have considered the $d_0/d_{\pi/4}$ junction: by using Ginzburg–Landau theories (Sigrist *et al* 1995, Östlund 1998) or quasiclassical Green's function techniques (Yip 1995, 1997, Fögelstrom *et al* 1998, Fögelstrom and Yip 1998), or by solving the Bogoliubov–de Gennes equation (Huck *et al* 1997, Zagoskin 1997, Zagoskin and Oshikawa 1998, Löfwander *et al* 2000). However, the final results are qualitatively the same: the π-periodic current–phase relation and the possibility of spontaneous TRSB. There is however one important difference: the absence (as above) or presence of a subdominant component of the order parameter at the junction. We conclude that broken time-reversal symmetry at a $d_0/d_{\pi/4}$ Josephson junction will not give any evidence for the presence of a subdominant component, since the d-wave order parameter alone enforces broken symmetry.

In experiments reported by Kirtley *et al* (1995a) and Mannhart *et al* (1996a) fractional fluxes were found at grain boundaries (GB) with the $d_0/d_{\pi/4}$ orientation. If time-reversal symmetry is broken as described above, spontaneous surface currents offer a possible explanation for these experiments; see (Sigrist (1998). However, Mannhart *et al* (1996a, b) proposed an explanation in terms of randomly distributed facets along the GB, where each facet may have equilibrium phase difference 0 or π depending on whether zero, one or two lobes with negative sign of the d-wave order parameter point towards the junction. When the phase difference varies along the GB, formation of fractional fluxes may be energetically favourable. It should be noted that this model assumes a simple $\sin\phi$ dependence of the current–phase relation, and does not take into account the formation of MGS at the junction.

3.2.7. d_0/d_0 junctions with resonant levels in the barrier. There is an interesting similarity between the Josephson effect in the $d_{\pi/4}/d_{\pi/4}$ junctions and in d_0/d_0 junctions with resonant states in the tunnel barrier. In the presence in the tunnel transparency of a narrow Breit–Wigner resonance close to the Fermi level, the Andreev level spectrum has the form found in the s-wave case (Beenakker and van Houten 1991, Wendin

and Shumeiko 1996b),

$$E = \pm\sqrt{E_0^2 + \Gamma^2 \cos^2(\phi/2)} \tag{25}$$

where E_0 is the position and Γ is the width of the resonance, $E_0, \Gamma \ll \Delta$. If the resonance is exactly at the Fermi level, $E_0 = 0$, the spectrum becomes

$$E = \pm\Gamma \cos(\phi/2) \tag{26}$$

which is the spectrum of an SNS junction ($D = 1$) with $|\Delta| = \Gamma$, having dispersion Γ instead of $|\Delta|$. At zero temperature, the current is then given by

$$j = \frac{e}{\hbar}\Gamma \sin\frac{\phi}{2}\,\mathrm{sgn}\left(\cos\frac{\phi}{2}\right). \tag{27}$$

The temperature dependence of the critical current in this case is then also $I_c(T) \propto 1/T$ for $k_BT \gg \Gamma$. Thus, while interpreting experimental results it is useful to have in mind that the low-temperature anomaly of the critical current is a fingerprint of a resonant state at the Fermi level rather than indication of the d-wave symmetry, although this resonance (MGS) could be due to the d-wave symmetry of the order parameter.

3.3. Critical Josephson current in GB and ramp–edge junctions

An important class of experimental studies involves the determination of the critical Josephson current in current-biased artificial GB junctions $\mathrm{d}_{\alpha_L}/\mathrm{d}_{\alpha_R}$ by varying the orientation angles α_L and α_R of the order parameters (Gross 1994, Delin and Kleinsasser 1996, Ivanov *et al* 1998, Arie *et al* 2000).

Consider a *gedanken* experiment where we may freely rotate the order parameters of the left (α_L) and right (α_R) superconducting electrodes, and also independently vary the transparency D of the interface barrier (I) (figure 5), creating ideal $\mathrm{d}_{\alpha_L}/\mathrm{d}_{\alpha_R}$ junctions: how will the Josephson current develop in different situations?

Starting with an ideal $\mathrm{d}_0/\mathrm{d}_0$ GB junction, there are no MGS, and the Josephson current $\propto D$ is due to non-resonant transport through the interface barrier. If we now rotate the order parameter symmetrically away from $\alpha = 0$ to $\alpha = \pi/4$, keeping D fixed, the $\mathrm{d}_\alpha/\mathrm{d}_{-\alpha}$ junction will develop MGS, and the critical current will then cross over from D to $\sqrt{D}$ dependence because of resonant transport through MGS. The resulting current enhancement can become very large ('giant Josephson current') if the transparency is low, $D \ll 1$, and the I_cR_N product will be enhanced by $1/\sqrt{D}$ over the Ambegaokar–Baratoff limit, characterizing $\mathrm{d}_0/\mathrm{d}_0$ tunnel junctions.

In reality, one must rotate the order parameter by rotating the lattice. This necessarily leads to an interface barrier, the strength of which increases with misorientation angle (up to $2\alpha = \pi/4$ for tetragonal symmetry). Assuming that the thickness of the barrier increases with misorientation angle, the result will be exponentially decreasing transparency and narrowing of the tunnelling cone. With decreasing transparency, the low-temperature region where MGS are important will decrease ($k_BT \propto \sqrt{\langle D\rangle}\Delta_0$ for resonant MGS). These effects may seriously reduce the weight of the MGS contribution. Therefore, in real experiments, the role of MGS will depend on the detailed properties of the junction.

It should be noted that if we continue to rotate the structure with the order parameters to reach the $\mathrm{d}_{\pi/4}/\mathrm{d}_{-\pi/4}$ limit, there is no longer any lattice mismatch, and therefore no interface barrier. The full presence of MGS therefore cannot be achieved in this type of experiment: to really observe the effects of MGS, one must fabricate $\mathrm{d}_{\pi/4}/\mathrm{I}/\mathrm{d}_{-\pi/4}$ junctions with separately controlled tunnel barriers.

In real high-T_c GB junctions, the I_cR_N product decreases strongly with increasing misorientation angle. In the absence of MGS, one would expect this product to be constant, but it is experimentally often found that $I_cR_N \propto 1/\rho_N$, where ρ_N is the normal resistance per unit area (Gross 1994). An explanation, due to Gross (1994), is that Coulomb blockade prevents resonant Josephson current but allows resonant normal current transport through the levels in the barrier. We suggest that this behaviour can also be explained in terms of a constant spectral density of normal levels with resonance widths Γ inside the barrier. From the discussion in section 3.2.7, we know that for a resonance with energy $E_0 \ll \Gamma$, equation (27) gives a resonantly enhanced Josephson current $I \propto \Gamma$, while for resonances with $E_0 \gg \Gamma$ the current is negligibly small. The contribution to the total current then comes from a spectral region of width Γ around $E = 0$, with the results $I \propto \Gamma^2$. The normal current, on the other hand, is resonantly enhanced in the entire spectral region, giving $I_cR_N \propto \Gamma \propto 1/\rho_N$.

In a recent paper, Arie *et al* (2000) have investigated the properties of the Josephson current in ramp–edge junctions with $\alpha_R - \alpha_L = \pi/4$ overall misorientation angle, varying the orientation of the interface (and therefore α_R, α_L) to vary the role of MGS. In particular, the dependence of the critical current on temperature has been experimentally investigated and fitted to d-wave theoretical results for short d/d junctions with high transparency, $D = 0.5$–0.8, which implies that the dispersion of the MGS is a large fraction of the gap. To get agreement with experiment for $T \to 0$, Arie *et al* (2000) introduced life-time broadening of the MGS (describing effects of rough interfaces and inelastic scattering) via an imaginary part of the energy, which strongly reduces $I_c(T)$ and the I_cR_N product at low temperatures, changing the sign of the curvature and leading to saturation of $I_c(T)$. The final good qualitative agreement between theory and experiment is consistent with the presence of life-time broadened MGS in a high-transparency junction.

It should be noted, however, that even if the transparency for superconductive transport seems high, an estimate of the experimental *average* transparency, based on the junction resistance (0.2–0.8 Ω) and area (number of planes and transport channels), gives a fairly low value, around $D = 10^{-3}$–10^{-4}. We suggest that the simplest explanation for this difference is that transport takes place through highly transparent point contacts in the junction barrier. In this picture, the temperature dependence of the critical Josephson current becomes a measure of the true transparency ($D \approx 1$), which together with the normal resistance also becomes a measure of the effective transport area of the junction.

For a more definitive analysis it is desirable to compare experimental and theoretical results for a larger set of

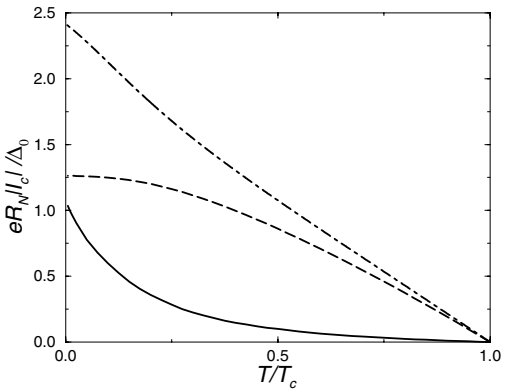

Figure 10. $I_c(T)$ dependences for high transparency, $\langle D\rangle = 0.68$ ($Z = 0.5$), for three orientations: d_0/d_0, dashed curve; $d_{\pi/4}/d_{-\pi/4}$, dash–dotted curve; and $d_{-15^\circ}/d_{30^\circ}$ full curve. The last orientation corresponds to the nominal orientation in the experiment by Arie *et al* (2000).

misorientation angles and transparencies. To this end we have calculated $I_c(T)$ for high transparency, $\langle D\rangle = 0.68$ ($Z = 0.5$, as in the original fit by Arie *et al* (2000)), neglecting MGS broadening. We have considered the high-symmetry orientations d_0/d_0 and $d_{\pi/4}/d_{-\pi/4}$, as well for the intermediate orientation d_{-15^0}/d_{30^0} considered by Arie *et al* (2000). The result is shown in figure 10. In the case of d_0/d_0 orientation (no MGS) we find that $I_c(T)$ has a weak negative curvature, while in the case of $d_{\pi/4}/d_{-\pi/4}$ orientation (MGS is present) we find a weak positive curvature of $I_c(T)$. Thus, within our model the positive curvature is characteristic for the presence of MGS, while the negative curvature is characteristic for the absence of MGS. The strong positive curvature in the case of the d_{-15^0}/d_{30^0} orientation in figure 10 may look a bit surprising: in fact, only at low temperatures does the $1/T$ dependence signify MGS; at higher temperatures it results from a competition between the nearly-linear MGS contribution and contributions of opposite signs from the continuum and gap–edge states. Thus, theoretically, positive curvature of $I_c(T)$ at low temperatures is a fingerprint of MGS. However, such a picture needs to be verified by systematic experimental and theoretical investigations, and the picture may be complicated. For example, the recent studies of GB junctions by Tafuri *et al* (1999) show clear positive $I_c(T)$ curvatures for nominally d_0/d_0 orientations, and such behaviour is also evident in the review by Delin and Kleinsasser (1996), perhaps due to orientational disorder like meandering and faceting.

Arie *et al* (2000) also studied the magnetic field depencence of the critical Josephson current, finding evidence for $\sin(2\phi)$ behaviour. This might be evidence for $d_0/d_{\pi/4}$ symmetry, but may also be due to the high transparency (saw-tooth-like dependence of the $I(\phi)$ current–phase relation).

We conclude that so far, the role of well defined MGS is difficult to identify with certainty in studies of the critical Josephson current in d/d GB or ramp–edge junctions, although Arie *et al* (2000) most likely have taken an important step in the right direction. In order to observe the presence of MGS one may have to use low-transparency tunnel junctions and utilize energy-resolving probes, for example looking for MGS in the form of characteristic features in I–V characteristics of voltage biased junctions.

4. Voltage-biased N/d junctions

Since the discovery of tunnelling in NS junctions (Giaever 1960), and the explanation of the phenomenon on the basis of the tunnel Hamiltonian model (Bardeen 1961, Cohen *et al* 1962), it is commonly accepted that the tunnelling conductance essentially measures the superconductor DOS. Hence, tunnel spectroscopy provides a direct means of detecting the MGS, which should show up as a large conductance peak centred at zero bias. This zero-bias conductance peak (ZBCP) has indeed been observed, see Geerk *et al* (1988), Kashiwaya *et al* (1995), Covington *et al* (1997), Ekin *et al* (1997), Alff *et al* (1997), Wei *et al* (1998), Aprili *et al* (1998a, b, 1999), Sinha and Ng (1998), Suzuki *et al* (1999), Krupke and Deutscher (1999), Wang *et al* (1999), Covington and Greene (2000) and references therein. See also the recent reviews by Alff and Gross (1999) and Kashiwaya and Tanaka (1999, 2000).

We start this section by discussing the theory of tunnelling through MGS. We will discuss two different transport mechanisms: direct tunnelling, and tunnelling involving Andreev reflection. The tunnel model is usually exploited for calculation of direct tunnelling, while Andreev reflection is usually described by means of scattering theory. We will compare the two approaches and show that depending on the relation between the junction transparency and the MGS intrinsic broadening, the MGS resonance may appear either in the single particle current or in the pair current. In the end we discuss tunnel experiments on NS junctions and also the recent STM investigations of impurity bound states.

4.1. Theoretical model

In the tunnel model, the angle-resolved local density of states (LDOS) ρ_L and ρ_R are calculated on the left (L) and right (R) sides of the junction, and then the tunnel formula

$$I(V,\theta) \propto \int_{-\infty}^{\infty} \mathrm{d}E\, D(\theta)[n_F(E) - n_F(E+eV)] \times \rho_L(\theta, E)\rho_R(\theta, E+eV) \tag{28}$$

is employed to calculate the current. The total current is obtained by angle integration $I(V) = \langle I(V,\theta)\rangle$, and the conductance is then found by differentiation with respect to the bias voltage V. Since the DOS in the normal metal is approximately energy independent near the Fermi surface, in the zero temperature limit the conductance will be reduced to $\langle D\rho_s(eV)\rangle$, where ρ_s is the LDOS in the superconductor.

For the $\alpha = 0$ orientation of the order parameter, there is no MGS and the angle resolved LDOS is the same as in the bulk $\rho_s \propto |E|/\sqrt{E^2 - |\Delta|^2}\Theta(|E| - |\Delta|)$ (see, for example, Matsumoto and Shiba (1995c) and Barash *et al* (1995)). The tunnel formula gives a conductance which in the zero temperature limit is simply the bulk DOS corrected by the angle-dependent transparency $D = D(\theta)$ of the tunnel barrier,

$$G(V) \propto \left\langle D\frac{eV}{\sqrt{eV^2 - |\Delta|^2}}\Theta(eV - |\Delta|)\right\rangle. \tag{29}$$

For other orientations, the conductance will measure LDOS at the surface rather than the bulk DOS. For the $\alpha = \pi/4$

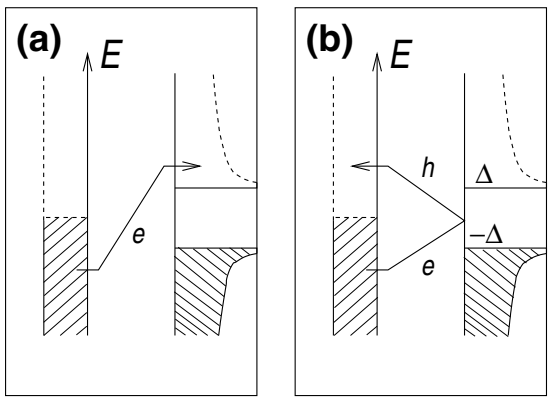

Figure 11. Illustration of (a) the single-particle (quasiparticle) and (b) the two-particle (Andreev) processes in the NIS junction. At zero temperature allowed processes connect occupied states below zero energy (the Fermi level) in the normal metal with (a) unoccupied states above the gap in the superconductor, and (b) above zero energy in the normal metal. We have aligned the Fermi energies of the two sides by a gauge transformation in the right superconductor; consequently, quasiparticles are accelerated by eV at each passing through the junction region.

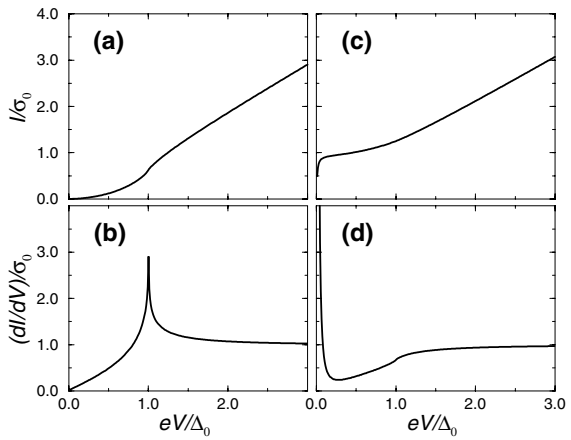

Figure 12. Current–voltage relations and corresponding differential conductances for the N/d_α junction with two different orientations: $\alpha = 0$, shown in (a) and (b), and $\alpha = \pi/4$, shown in (c) and (d). The zero-bias anomaly in (c) and (d) is due to the MGS resonance. The barrier is modelled by a δ-function potential with a large tunnel cone with angle averaged transparency $\langle D\rangle = 0.026$, which emphasize the importance of the MGS resonances that appear for finite injection angles θ only. The temperature is zero and σ_0 is the normal state conductance.

orientation, neglecting gap suppression and surface roughness, the LDOS is given by (Matsumoto and Shiba 1995c)

$$\rho_s(\theta, E) \propto \frac{\sqrt{E^2-\Delta^2}}{|E|}\Theta(|E|-|\Delta|) + \pi|\Delta|\delta(E). \quad (30)$$

The high spectral weight at the gap edges has moved down to zero energy and formed the MGS, and the tunnel conductance will contain a peak at zero voltage. The delta-function singularity is usually removed by introducing broadening via an imaginary part η of the energy representing some relaxation mechanism. This damping η determines the width of the MGS resonance.

This interpretation of the conductance spectra in terms of single-particle (quasiparticle) current, see figure 11(a), assumes that all states in the electrodes form reservoirs, i.e. their relaxation times are assumed short enough to ensure equilibrium. This assumption is reasonable for the extended states of the continuum, while for the MGS, lying deep within the superconducting gap, it requires special consideration. If the MGS are true bound states without coupling to the bulk of the superconductor, i.e. intrinsically very narrow, then current transport through the MGS is only possible via the Andreev process; see figure 11(b). The equation for the current then reads

$$I(V) = I_1(V) + I_2(V) \quad (31)$$

where I_1 and I_2 are the single-particle (quasiparticle) and two-particle (Andreev) currents, respectively. This case of narrow MGS is most easily studied within the scattering approach (Landauer 1957, Büttiker 1986, Imry 1986).

Blonder *et al* (1982) were the first to use scattering theory to calculate the conductance of an s-wave NS junction. Later on, Bruder (1990), Kashiwaya *et al* (1995) and Xu *et al* (1996) generalized the theory to the d-wave case; see also Tanaka and Kashiwaya (1995, 1996b) and Kashiwaya and Tanaka (1996). At zero temperature, in the low-transparency limit, we have for the $\alpha = \pi/4$ orientation

$$I_1(\theta, E) = D\frac{\sqrt{E^2-\Delta^2}}{|E|}\Theta(|E|-|\Delta|) \quad (32)$$

and the two-particle current takes the form

$$I_2(\theta, E) = \frac{2D^2}{D^2 + 4R(E/\Delta)^2}. \quad (33)$$

The total current is obtained by integration over angles and energies

$$I(V) \propto \left\langle \int_{-\infty}^{\infty} \mathrm{d}E[n_F(E) - n_F(E+eV)][I_1(\theta, E) + I_2(\theta, E)] \right\rangle. \quad (34)$$

The two-particle current contains a Breit–Wigner resonance of width $\Delta D/2\sqrt{R}$, the MGS, and $I_2 \propto \Delta D$ as soon as $eV > \Delta D$. Hence, the two-particle current is resonantly enhanced near zero bias (it is of the same order as the single-particle current), which produces a zero-bias conductance peak. The current–voltage and conductance–voltage relations calculated within the scattering approach are plotted in figure 12.

Consider now the ratio q between the life time due to leakage to the normal reservoir through the barrier, $\tau_b \propto \hbar/\Delta_0 D$, and the life time due to inelastic relaxation, $\tau_r \propto \hbar/\eta$, which couple the MGS with the bulk superconductor,

$$q = \frac{\tau_b}{\tau_r} \propto \frac{\eta}{\Delta_0 D}. \quad (35)$$

Clearly this life-time ratio will determine whether the MGS will participate in current transport via the single-particle process (for large damping; $q \gg 1$), or via the two-particle process (for small damping; $q \ll 1$).

The fingerprint of Andreev transport is the so-called excess current defined as (Artemenko *et al* 1979)

$$I_{exc} = \lim_{V\to\infty}[I_S(V) - I_N(V)] \quad (36)$$

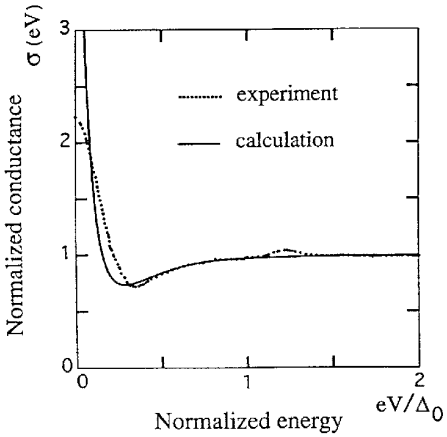

Figure 13. Conductance spectra, normalized by the normal background conductance, obtained on YBCO at 4.2 K by STM fitted by the scattering theory of MGS, assuming the $\alpha = \pi/4$ orientation. The parameters of the theory are the maximum d-wave gap $\Delta_0 = 17.8$ meV, the normalized barrier height $Z = 2mH/\hbar^2 k_F = 3$ (H is the height of the barrier potential), and tunnel cone parameter $\beta = 10$, (from Kashiwaya *et al* (1995)).

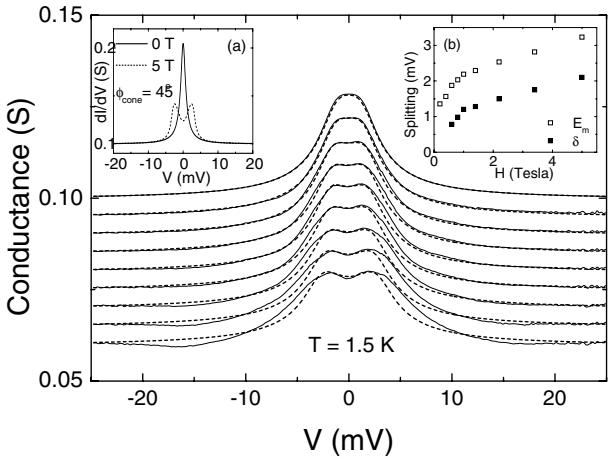

Figure 14. Demonstration of the Doppler shift of MGS in the presence of a magnetic field $H = \{0.2, 0.4, 0.6, 0.8, 1.0, 2.2, 3.4, 5.0\}T$ in YBCO/Pb junctions, where the curve at the top is for the lowest field. The spectra are normalized by the high-voltage conductance at $H = 0.2T$ and fitted by a Lorentzian centred at the bound states energy $E_B = v_F p_s \cos\theta$ averaged over angles θ with a tunnel cone $D(\theta) = 1$ for $|\theta| < \theta_c = 15^\circ$ and $D(\theta) = 0$ otherwise. The fit parameters are the Lorentzian width $\Gamma = [\Delta_0/\Delta(\theta)] \times 0.8$ meV and $v_F p_s$. In inset (a) theoretical results are shown for a larger tunnelling cone for comparison. In inset (b) the maximum Doppler shift $E_m = v_F p_s \cos(\pi/2 - \theta_c)$ and the ZBCP splitting δ are both shown as a function of applied field H, (from Aprili *et al* (1999)).

where I_S and I_N are the currents in the superconducting and normal states, respectively. Following the work of Blonder *et al* (1982), it became common practice to estimate the efficiency of Andreev reflection from the magnitude of the excess current. Since in the present case $I_2 \sim D$, one would expect that also $I_{exc} \sim D$. However, it can be shown that the single-particle current gives a large negative contribution to the excess current: this cancels the enhanced two-particle current and leaves an excess current which for all orientations is proportional to D^2 in the low-transparency limit, just like in the low-temperature superconductors. This implies that the excess current will not be a true measure of the importance of the Andreev reflection process as soon as there are resonances (like the MGS) in the junction.

4.2. Experiments

Experimentally, the ZBCP has been studied for many years: it had already been observed by Geerk *et al* (1988). In the early years, when the d-wave symmetry of the order parameter had not been established, the peak was explained in terms of a spin-flip scattering model developed by Appelbaum (1966) and Anderson (1966). Following the paper by Hu (1994), attention was drawn to the MGS scenario. One of the first good fits between experiments and the d-wave theory (MGS, figure 13) was presented by Kashiwaya *et al* (1995). Today, a number of experiments have given quite convincing evidence that the MGS picture offers the best explanation. Here we shall discuss some experimental findings regarding the influence of (1) magnetic field and (2) orientation and disorder on the MGS and ZBCP. Yet another class of experiments have been performed recently, namely STM measurements of MGS bound to point impurities. These experiments will be discussed in section 4.2.3 below.

4.2.1. Magnetic field. The Doppler shift effect mentioned in section 2.2 was confirmed experimentally by Covington *et al* (1977) and may be regarded as the first successful attempt to seriously discriminate between the MGS and the spin-flip scattering scenarios for the ZBCP. The effect was further studied by Krupke and Deutscher (1999) and Aprili *et al* (1999); see figure 14. The ZBCP was observed to split linearly with H up to H_{c1}, where vortices enter the superconductor and the shift saturates (Fogelström *et al* 1997). It was pointed out that the spin-flip model could be ruled out since the Landé g-factor involved in the Zeeman-type splitting in this case had to be very large in order to fit the experiment.

In the zero-field limit $H \to 0$, splitting of the ZBCP was still observed by Covington *et al* (1997) and Krupke and Deutscher (1999) and also by Kashiwaya *et al* (1998b) and Lesueur *et al* (1999). This was interpreted as a sign of spontaneous TRSB at the surface and evidence for a local presence of a subdominant s-wave component; see section 2.2. However, a spontaneous (zero-field) splitting of the ZBCP is not always seen (Aprili *et al* 1999, Yeh *et al* 2000). Moreover, there are other possible explanations for the splitting than that involving a subdominant s-wave component of the order parameter; see the discussion of split MGS in section 2.6. Also, if for any reason particle–hole symmetry is broken in the superconductor, the MGS may also be split. For the identification of the mechanism responsible for the spontaneous splitting of the ZBCP the same arguments as for the identification of the origin of the ZBCP are relevant: one needs to measure the response to some controllable perturbation; for example the magnetic field response of the ZBCP discussed above confirmed that MGS are responsible for the ZBCP. Since such experiments are lacking for the spontaneously split ZBCP, we feel that at the present time the existence of a TRSB $d + is$ surface state remains controversial.

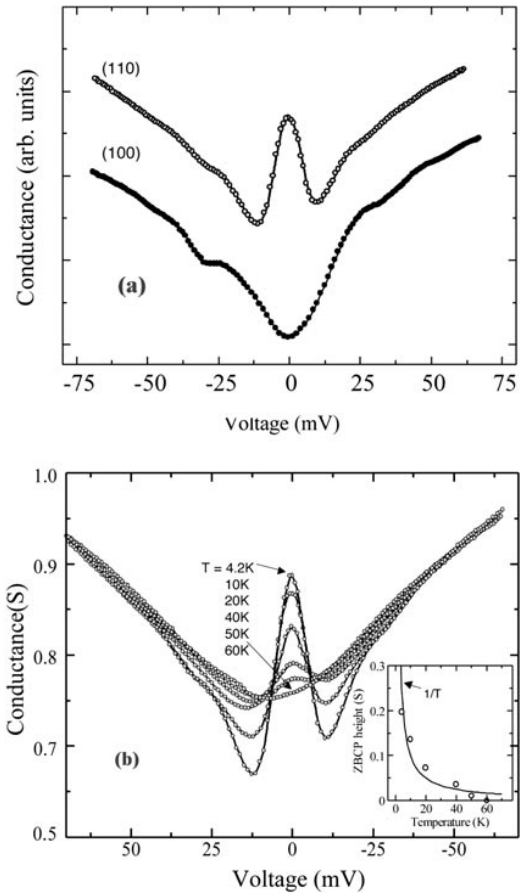

Figure 15. (a) Conductance of YBCO/Ag ramp–edge junctions showing the orientation dependence of the zero-bias conductance peak as predicted by the MGS scenario: for $\alpha = 0$ the peak is absent (the (100) curve), while it is present for the $\alpha = \pi/4$ orientation (the (110) curve). (b) Temperature dependence of the conductance peak (the (110) curve in (a)). The peak height scales as $1/T$, as shown in the inset, while the width is temperature independent, (from Wang *et al* (1999)).

4.2.2. Orientation. As explained above, if we probe an $\alpha = \pi/4$ surface (i.e. [110] surface) a large ZBCP should be present, while if we probe an $\alpha = 0$ surface (i.e. [100] or [010] surfaces) the ZBCP should be absent. In some well controlled measurements (Alff *et al* 1997, Wei *et al* 1998, Wang *et al* 1999, Iguchi *et al* 2000) it has been verified that the ZBCP has this orientation dependence (see figure 15). However, because of junction inhomogeneities like faceting (Fogelström *et al* 1997), the local orientation at the junction may not be well defined. For example the planar junction experiments performed by Covington *et al* (1997) showed equal weight of the ZBCP for all orientations of the electrodes.

Aprili *et al* (1998) studied broadening effects on the ZBCP due to impurities introduced into the junction via ion bombardment. The result suggests that disorder introduces decoherence which removes the MGS resonance. Aprili *et al* (1998) argue that if the spin-flip mechanism were responsible for the ZBCP, the disorder should not have such a large impact, indicating that the MGS are responsible for the ZBCP.

Figure 15 shows that the peak height decreases with $1/T$ while the width seems to remain roughly constant, independent of temperature. This information is obtained by assuming

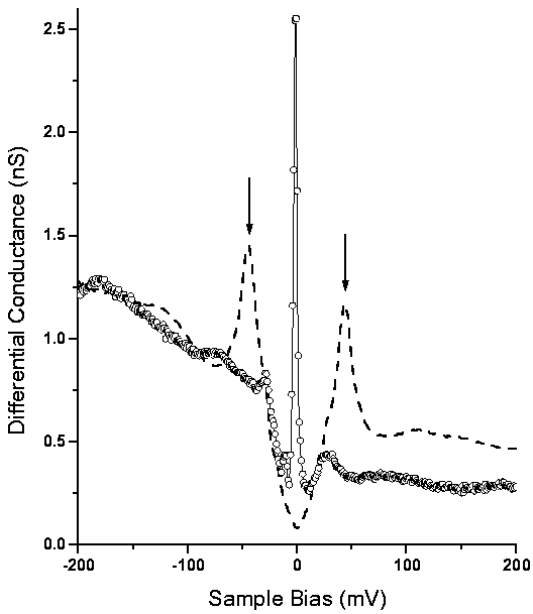

Figure 16. Conductance spectra of Zn-doped BSCCO obtained by STM in the *c*-axis direction at 4.2 K. The spectrum taken at a Zn impurity site contains a huge zero-bias anomaly (open circles), while the spectrum taken at a clean region is of the usual d-wave form with peaks at the gap voltages (arrows), (from Pan *et al* (2000a)).

that the peak is positioned on a background in the form of a temperature-dependent gap. In that case, the FWHM is roughly the distance between the two 'fix points' in figure 15. This behaviour implies that the density of MGS (the area of the peak) decreases with increasing temperature, which cannot be explained by thermal smearing. The question of temperature-independent width has been addressed by Walker and Pairor (1999) in terms of the effect of rough interfaces and surface umklapp scattering.

4.2.3. Impurity induced MGS. Bound states induced by impurities have been found experimentally by different groups (Yazdani *et al* 1999, Hudson *et al* 1999, Pan *et al* 2000a). In the most recent experiment by Pan *et al* (2000a) the LDOS was measured by STM in the vicinity of a single impurity (Zn) replacing a Cu atom in the superconducting plane of $Bi_2Sr_2CaCu_2O_{8+\delta}$ (BSCCO) (figure 16). It was found that the LDOS is enhanced at low energy and it has an anisotropic form in real space. This observation is in qualitatively good agreement with theoretical predictions; see Balatsky *et al* (1995), Balatsky and Salkola (1996), Salkola *et al* (1996), Flatté and Byers (1998), Zhu *et al* (2000a, b), Haas and Maki (2000) and references therein. It was predicted that a point-like impurity in a d-wave superconductor is able to form a resonant state within the superconducting gap. If global particle–hole symmetry is present, then in the unitary limit (strong impurity potential), the energy of the resonance approaches the Fermi level, and the resonance width tends to zero, the MGS becoming a true bound state.

We can understand this effect by considering a defect with a hard specular boundary the size of which is much larger than the coherence length, as discussed by Matsumoto *et al* (1997). In this case, the defect surface can be locally

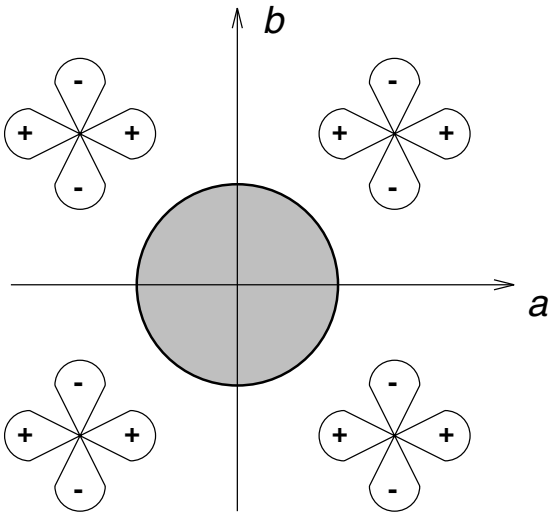

Figure 17. The *local* orientation at a circular impenetrable extended impurity in a two-dimensional d-wave superconductor favours the formation of MGS. In real space the wavefunction leaks out along the gap nodes, shown in the figure, giving a cross shaped density of states similar to what was observed in the experiments by Pan *et al* (2000a).

approximated by a planar surface, and our arguments in favour of the presence of the MGS holds. Since different parts of the defect boundary have different orientations with respect to the crystallographic axes and continuously change from $\alpha = 0$ to $\alpha = 2\pi$, there are different amounts of trajectories containing local MGS. Consider, for example, a circular defect, as illustrated in figure 17. Then for the (110) and (-110) directions the local angle is $\alpha = \pi/4(1+2n)$ which corresponds to a maximum amount of MGS trajectories, while for (100) and (010) orientations, the local angle is $\alpha = n\pi/2$ which corresponds to a minimum amount of MGS trajectories. Hence, the LDOS at low energy (Mastumoto *et al* 1997) is cross shaped in space with tails along the nodes. The density of states decreases far from the defect because the MGS are localized near the scatterer over a distance of the order of the coherence length.

In fact, the above arguments rely entirely on quasiclassical dynamics of superconducting quasiparticles, and can therefore be extended (see appendix A4) to defects smaller than the coherence length but larger than the Fermi wavelength (Adagideli *et al* 1999). However, in high-T_c materials this difference is not that important since the coherence length is rather small.

At the time of writing, an issue under debate is whether the impurity MGS are localized or extended; see, for example, Zhu *et al* (2000c). In a large crystal there are many impurities, or inhomogeneities, and hence many MGS, which in principle can form an impurity band similar to impurity bands in semiconductors. In simplified terms, the MGS wavefunction can leak out along the gap nodes (the cross-shaped DOS described above); if wavefunction overlaps between neighbouring impurity states are significant, an impurity band may form. Also experimentally, the issue is controversial. Thermal conductivity measurements (Taillefer *et al* 1997, Behnia *et al* 1999) on Y123 and BSCCO indicate the existence of extended quasiparticle states, while other investigations (Hussey *et al* 2000) on under-doped Y124 indicate the opposite.

5. Voltage-biased d/d junctions

In this section we study the ac Josephson effect in superconducting junctions. We begin by outlining the microscopic theory of charge transport in voltage biased Josephson junctions. Then we discuss how the MGS resonance appears in this case. In particular, we show that depending on the life-time ratio q introduced in the previous section, the MGS resonance appears either in the pair current at the gap voltage $eV = \Delta$ (for small intrinsic broadening, $q \ll 1$), or in the single particle current both near zero voltage and at the gap voltage (for large intrinsic broadening, $q \gg 1$). At the end of the section we discuss some experiments.

5.1. Theoretical formulation

Generalization of the previous theory of transport through N/d junctions to d/d junctions (beyond the tunnel model; equation (28)) is non-trivial due to the Josephson effect. In the presence of a bias voltage, the phase difference over the Josephson junction becomes time dependent, $\partial_t \phi = 2eV/\hbar$ (Josephson 1962), and a quasiparticle incident on the junction will see the junction as a scatterer whose properties periodically change in time with the Josephson frequency $\omega_J = 2eV/\hbar$. In the limit of small applied voltage, $eV \ll \Delta$, the time-dependent current can be understood via adiabatic arguments, in terms of a time-dependent phase, letting $\phi \to \phi(t) = 2eVt/\hbar$ in the equation for the dc Josephson current (Averin and Bardas 1995, Bratus' *et al* 1997). In the general case, a full quantum mechanical consideration is necessary for inelastic scattering by the time-dependent scatterer, taking into account transitions between the incident quasiparticle energy E and an infinite set of sideband energies $E_n = E + neV$ (n are integers). The time-dependent current can then be decomposed into a spectrum of frequency components

$$I(V,t) = \sum_{m=-\infty}^{\infty} I_m(V)\, \mathrm{e}^{\mathrm{i}m\omega_J t}, \qquad I_{-m}(V) = I_m^*(V) \quad (37)$$

where the $m = 0$ component is the time averaged current and the $m \neq 0$ components correspond to the ac oscillations with basic frequency $\omega_J = 2eV/\hbar$. Interestingly, the very early observation by Estève *et al* (1987) of the ac Josephson effect was taken as one of the first proofs for the existence of Cooper pairs in the high-T_c superconductors.

Within the adiabatic picture for the d-wave junctions, the π-periodic current–phase relation in the $\mathrm{d}_0/\mathrm{d}_{\pi/4}$ junction (see figure 9) will result in an ac Josephson oscillation with twice the usual frequency, $2\omega_J$. This was predicted by Yip *et al* (1990, 1993) and Zagoskin (1997) using the adiabaticity arguments, and it was recently confirmed by a full calculation of equation (37) by Löfwander *et al* (1998). Possibly this effect was observed in experiments by Early *et al* (1993), although the authors presented an alternative explanation in terms of parallel junctions in the grain boundary.

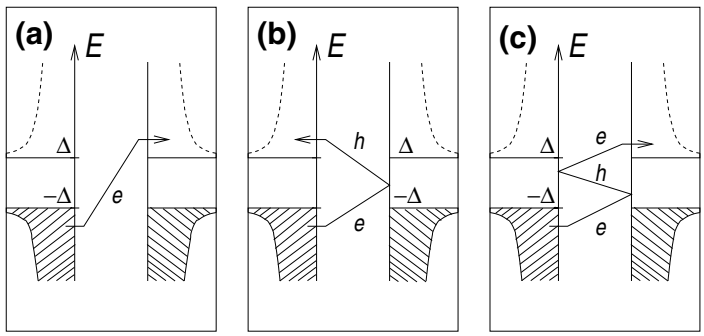

Figure 18. Illustration of the (a) single-particle, (b) two-particle, and (c) three-particle processes in the SIS junction. At zero temperature allowed processes connect occupied states below the gap in the left superconductor with unoccupied states above the gap in the superconductors. We have aligned the Fermi energies of the two sides by a gauge transformation in the right superconductor; consequently, quasiparticles are accelerated by eV at each passing through the junction region.

The time-independent ($m = 0$) current, from now on called the dc current, has contributions from all sidebands, $-\infty < E_n < \infty$, and at low temperature it has the form

$$I_{dc}(V) = \sum_{n=1}^{\infty} I_n^{dc}(V). \tag{38}$$

Remarkably, this expansion for the dc current has two different physical interpretations, which in fact are equivalent, namely multiparticle tunnelling (MPT) and multiple Andreev reflection (MAR). A consistent theory unifying the concepts of MPT and MAR has been presented by Bratus' *et al* (1995) and Shumeiko *et al* (1997).

The first interpretation, MPT, is particularly useful in the tunnel limit, $D \ll 1$. It was originally suggested by Schrieffer and Wilkins (1963) using perturbative tunnel model calculations, and it was improved by Cuevas *et al* (1996). According to this interpretation the $n = 1$ current, $I_1^{dc}(V)$, is due to single-particle tunnelling processes, and it corresponds to the quasiparticle current in a standard tunnel model calculation. The $n = 2$ current, $I_2^{dc}(V)$, is due to two-particle tunnelling processes which have smaller probability, $\sim D^2$, and so on. In s-wave junctions, energy conservation prohibits the n-particle tunnelling process for $neV < 2\Delta$. Thus, each n-particle current has a threshold at voltage $eV_n = 2\Delta/n$ and the magnitude of this current is proportional to D^n. However, resonances due to the presence of surface states or resonances in the barrier may lower the exponent and enhance the intensity of the process (Johansson *et al* 1999a, b).

The second interpretation, more useful for transparent junctions, is based on the scattering theory and involves MAR (Klapwijk *et al* 1982, Arnold 1987, Bratus' *et al* 1995, Averin and Bardas 1995). According to this interpretation, the current $I_1^{dc}(V)$ is due to direct scattering (acceleration) across the energy gap (see figure 18(a)), while the current $I_2^{dc}(V)$ is due to the Andreev reflection processes, in the same way as in the NS junction, equation (31), depicted in figure 18(b). For smaller voltage, the Andreev reflected hole may be Andreev reflected once more when reaching the left superconductor, this time as an electron (see figure 18(c)), giving the current $I_3^{dc}(V)$, and so on. The multiple Andreev reflections form, in principle, an infinite series of currents, equation (38). The magnitude of each current is proportional to D^n (in the absence of resonances), since each process contains n coherent passages through the barrier.

The equivalence of these two interpretations—MPT and MAR—is due to the fact that at every Andreev reflection one pair of electrons is transmitted through the SN interface, and therefore the MAR process with n Andreev reflections transfers a charge $(n + 1)e$, corresponding to the $n + 1$-particle current (Arnold 1987, Shumeiko *et al* 1997).

In s-wave junctions, the onsets of the n-particle currents at $eV = 2\Delta/n$, together with peaks at the same voltages in the higher order currents due to the DOS peaks near the gap edges, is the explanation for the so-called subharmonic gap structure (SGS); see Ludoph *et al* (2000) and references therein.

In d-wave superconductors, the subgap structure (Hurd 1997, Barash and Svidzinsky 1997, Hurd *et al* 1999, Löfwander *et al* 1999a, b, Samanta and Datta 1998, Yoshida *et al* 1999) is very different for two reasons: (1) the multiparticle current thresholds are washed out due to the gap nodes, (2) the presence of MGS changes the resonances in energy space. For the d_0/d_0 orientation (no MGS in the junction), the single-particle current dominates the I–V characteristics because of the gap nodes. Higher-order processes ($n \geqslant 2$) are very small corrections and can be neglected; thus, subharmonic gap structure at $eV_n = 2\Delta/n$ is suppressed in the I–V characteristics in d-wave junctions; see figure 19(a). When MGS are present in the junction, new resonances appear. In particular, the two-particle process becomes resonant (see below) and must be taken into account. Although the MGS may also enhance higher-order processes than $n = 2$, these resonances are always very weak compared to the two-particle process. For these reasons we will in the following only discuss the single-particle and two-particle currents.

We start our discussion of the I–V characteristics of junctions with MGS by presenting in figure 19(b)–(d) results of full numerical calculations of equation (38) for junctions where the right electrode has d-wave symmetry with orientation $\alpha_R = \pi/4$ and the left counter electrode has s-wave symmetry ($s/d_{\pi/4}$ junction), d-wave symmetry with $\alpha_L = 0$ orientation ($d_0/d_{\pi/4}$ junction), and d-wave symmetry with $\alpha_L = \pi/4$ orientation ($d_{\pi/4}/d_{\pi/4}$ junction), respectively. In the last junction case we introduced a small imaginary part (to model broadening) to the energy in order to reveal the current peak near zero bias. If the MGS are strongly coupled to the reservoirs (large intrinsic broadening, $q \gg 1$), the current–voltage characteristics in figure 19 are dominated by single-particle tunnelling, and

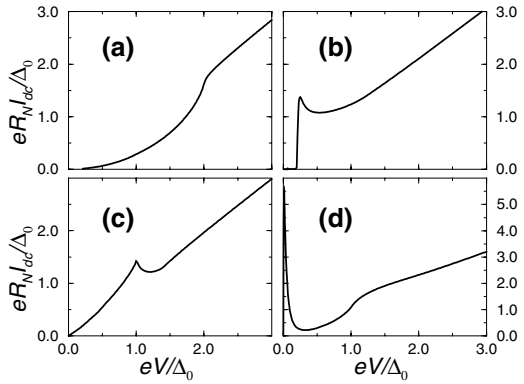

Figure 19. The total dc current in junctions with orientations (a) d_0/d_0, (b) $s/d_{\pi/4}$ where $\Delta_s = 0.2\Delta_0$ (Δ_s is the s-wave superconducting gap and Δ_0 is the maximum d-wave gap), (c) $d_0/d_{\pi/4}$, and (d) $d_{\pi/4}/d_{\pi/4}$. The transparency of the tunnel barrier is $\langle D\rangle = 0.026$ in all cases and we assume zero temperature.

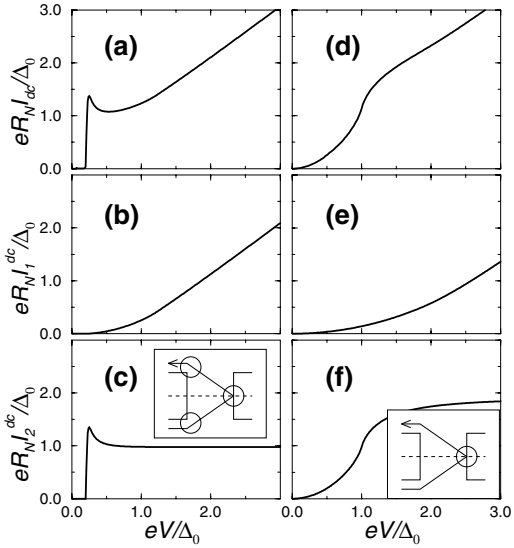

Figure 20. (a)–(c) The total current (the same curve as in figure 19(b)), the one-particle current, and the two-particle current in the $s/d_{\pi/4}$ junction with $\Delta_s = 0.2\Delta_0$ where Δ_s is the s-wave superconducting gap and Δ_0 is the maximum d-wave gap. The peak at the gap voltage is due to the MGS resonance on the right-hand side overlapping with the gap–edge resonances at the entrance and exit points on the s-wave superconductors side; see inset in (c) where the circles indicate presence of resonance. Equivalently, we can say that the large BCS gap–edge DOS pushes more current through the MGS, compared to the NS case. (d)–(f) The total current, the one-particle current, and the two-particle current in the $d_{\pi/4}/d_{\pi/4}$ junction. The onset at the gap voltage is due to the *bare* MGS resonance; see inset in (f) where the circles indicate presence of resonance. The transparency of the tunnel barrier is $\langle D\rangle = 0.026$ in all cases and we assume zero temperature.

they can be qualitatively understood by applying tunnel model arguments. Indeed, when the right superconductor is a d-wave superconductor with the $\pi/4$ orientation, the local density of states is given by equation (30); the MGS delta function $\delta(E)$ then produces a term (Samanta and Datta 1998)

$$I_1^{dc}(V) \propto \langle D(\theta)[n_F(-eV) - n_F(0)]\rho_L(\theta, -eV)\rangle. \quad (39)$$

Within this model, we understand figures 19(b)–(d) as simply the s-wave DOS, the angle integrated d-wave DOS, and finally the midgap peak. Note that the *current itself* rather than the conductance is proportional to the LDOS ρ_L of the left superconductor. For voltages $eV > \Delta$ terms not included in equation (39) become important and for $eV \gg \Delta$ the current is proportional to the applied voltage.

When the MGS are intrinsically very narrow ($q \ll 1$), the resonance will not appear in the single-particle current, instead the resonance appears in the two-particle current (compare the discussion of the N/d junction in section 4). We exemplify this with the $s/d_{\pi/4}$ and $d_{\pi/4}/d_{\pi/4}$ junction cases by plotting the single- and two-particle currents separately along with the total currents in figure 20. In the $s/d_{\pi/4}$ junction case, the I–V relations (total current) for the $q \gg 1$ and $q \ll 1$ cases are similar, although in the $q \ll 1$ limit the peak at the s-wave gap voltage is due to the two-particle current; the resonant process is shown in the inset. This situation is equivalent to the one in the N/d case discussed in section 4. However, in the $d_{\pi/4}/d_{\pi/4}$ junctions, which have MGS at both sides of the junction barrier, the situation is different. The process of MGS-to-MGS tunnelling is absent in the small q limit. Thus there is no current peak at small voltage in this case (compare figure 19(d) and figure 20(d)); instead the resonance shows up in the two-particle current at the gap-voltage $eV = \Delta$, see figure 20(f); the resonant process is shown in the inset. Thus, for this orientation it should be possible experimentally to distinguish the two cases, large or small q, by observing where the resonance appears: either near zero voltage ($q \gg 1$) or at the gap voltage ($q \ll 1$), respectively.

5.2. Comments on experimental results

A large number of current–voltage characteristics measurements have been performed with GB and ramp–edge junctions (Delin and Kleinsasser 1996). In this review we will not make any serious attempt to analyse these experiments beyond what is stated in the original papers. Instead we will make some comments on a few specific issues.

Measurements of the current–voltage characteristics of d/d junctions are difficult to analyse. Besides complications with the samples (see the discussion of measurements of the critical Josephson current in section 3.3), the presence of the Josephson effect makes the subgap voltage region hard to interpret.

Because of the Josephson current, an essential issue concerns how to measure current–voltage characteristics. In order to measure quasiparticle current and conductivity, and to observe the MGS zero-bias peaks, one must work with voltage bias, which by definition avoids the problem with the dc Josephson current. However, this is hard to do experimentally, because of the low junction impedance; in practice, current bias is therefore usually employed.

Alff *et al* (1998a, b) have recently reported current–voltage characteristic measurements on symmetric $d_\alpha/d_{-\alpha}$ HTS grain boundary junctions with large misorientation angles, in the range 30–45°. These junctions show very small or vanishing Josephson current, and the conductance dI/dV versus V shows a zero-energy structure quite similar to NIS junctions (see figure 15), with similar temperature and magnetic field dependences. Alff *et al* (1998a, b) conclude that they in fact observe NIS-like behaviour, although they interpret

the zero-energy structure in the $\mathrm{d}I/\mathrm{d}V$ versus V characteristic as a ZBCP resulting from an SIS convolution of density of states with strongly broadened MGS.

The similarity of the ZBCP of the NIS and SIS junctions is striking, and we would like to consider the following tentative explanation. For an SIS junction to behave like an NIS junction, it is necessary that there are very strong relaxation effects in the barrier region, the barrier acting as a reservoir, which results in decoupling of the two SI and IS interfaces. The SI/IS junctions will then be in series and each will be biased by $eV/2$; as a result, there will be a zero-bias onset of the current (without peak) as in the NIS junction, but the maximum gap should occur at 2Δ. The average gap voltage V_g could be well below this value. Whether this agrees with the experimental results remains an open question since there is no independent measurement of the gap in the experiment.

Alff *et al* (1998a, b) rather consider their results to signify that the junction is in the *tunnelling* regime, SIS, albeit tunnelling is considered to proceed through resonant states in the barrier. Let us then assume that we can describe the junction as a 'tunnel' junction S'I'S, where the 'I'-region cannot be regarded as a reservoir. The Josephson current could still be suppressed for several reasons: the junction could be long in comparison with the coherence length, or suppressed by inelastic interactions, or there could be fluctuations and noise causing the two sides of the junction to become incoherent. In a symmetric situation with narrow MGS on both sides of the junction, as described before, the MGS DOS peaks will then be convoluted, leading to a current peak, i.e. to a peak in the current–voltage characteristics and not in the conductance. In this view, the conductance zero-energy anomaly in the $\mathrm{d}_\alpha/\mathrm{d}_{-\alpha}$ junction describes the *voltage derivative* of the MGS DOS, and should not be directly compared with the MGS DOS of the NIS junction.

Note that if the MGS is very broad, say $\Gamma \sim 0.3\Delta_0$, the MGS peak in the calculated current–voltage characteristics will merge into the rising background, and the result may *appear similar* to the NIS case; nevertheless, in our opinion, one should still look for the MGS DOS in the current–voltage characteristics, and not in the conductance. However, with such extreme broadending the MGS may act as normal reservoirs in the gap, and the whole situation may have to be reconsidered.

In conclusion, we believe that further progress depends on close interaction between experiment and theory to critically examine models and results in order to produce internally consistent pictures and new critical experimental tests.

6. Other experiments

6.1. c-axis tunnelling

For a long time, the presence of a Josephson current in experiments on *c*-axis tunnel junctions between YBCO and Pb has been regarded as rather mysterious, because if the order parameter of YBCO has pure d-wave symmetry, the first order Josephson coupling should vanish, only leaving a small residual second-order current (see, for example, Sun *et al* (1994), Kleiner *et al* (1996) and Lesueur *et al* (1997)). This conclusion however relies on the assumption that the *c*-axis current injection, from, for example, an STM tip, results in a spherically symmetric *ab*-plane injection current. Only under such circumstances is the overlap between the s-wave and the d-wave order parameters zero. Considering spherical injection, the orthorhombic structure of YBCO indicates that there may be, in addition to the d-wave order parameter, a small s-wave component present which could be responsible for the first-order Josephson coupling observed in the experiments. However, twinning spoils this explanation since neighbouring twins should have different signs of the s-wave component, and the average Josephson current should be close to zero. Kouznetsov *et al* (1997) studied tunnelling along the *c*-axis from Pb into YBCO containing one single twin boundary. It was shown that indeed a $\mathrm{d} \pm s$ order parameter is realized in YBCO and that the sign between the d-wave and s-wave components is opposite on the two opposite sides of the twin boundary. However, also in experiments on junctions between Pb and highly twinned YBCO (Kleiner *et al* 1996), a first-order Josephson coupling was found. Furthermore, in experiments on *c*-axis BSCCO–Pb junctions (Mössle and Kleiner 1999) a finite first-order Josephson coupling was observed and interpreted in terms of a small s-wave component also in BSCCO. Recently an interesting possibility was brought forward by Rae (2000), who pointed out that Pb is a rather anisotropic s-wave superconductor and showed how this asymmetry on the s-wave superconductor side can explain at least the experiments on BSCCO. To test this idea, a thorough investigation of the Josephson coupling between isotropic s-wave superconductors and BSCCO should be performed.

6.2. Electron-doped cuprates

Very recently, Tsuei and Kirtley (2000b) found the half-flux quantum also in tricrystal rings of the electron-doped cuprates $Nd_{1.85}Ce_{0.15}CuO_{4-\delta}$ (NCCO) and $Pr_{1.85}Ce_{0.15}CuO_{4-\delta}$ (PCCO). This provides very strong evidence for d-wave superconductivity in both these materials. This conclusion is supported by the power-law dependence of the penetration depth found by Prozorov *et al* (2000). However, in transport experiments (Ekin *et al* 1997, Alff *et al* 1998b, 1999, Kashiwaya *et al* 1998a, Kleefisch *et al* 1998) ZBCP were never found. Instead, more or less V-shaped spectra were obtained. This absence of ZBPC was taken as evidence for an anisotropic s-wave order parameter in NCCO, but now turns out to be in disagreement with the very recent tricrystal ring experiments (Tsuei and Kirtley 2000). Therefore, at this point, a reexamination of the transport properties of the electron-doped materials seems necessary in order to check the presence of MGS in these materials. We would like to point out that the experimental results obtained by Alff can be understood within the MGS scenario if the MGS in these materials are intrinsically very narrow (small q, equation (35)). However, also in the normal-metal–superconductor (N/d) experiments on NCCO by Kashiwaya *et al* (1998a) the ZBCP was absent, which cannot be explained by a narrow MGS only.

7. Summary and concluding remarks

MGS are consequences of the angle-dependent sign change of the order parameter and provide direct evidence for d-wave

symmetry. Transport measurements which detect the MGS resonance at the Fermi energy for particular orientations of the plane of the junction with respect to the crystallographic axes will provide crucial evidence for d-wave superconductivity. The MGS phenomenon is part of a general problem of superconducting surface and interface states and their relation to the Andreev states, which determine the transport properties of superconducting junctions.

Surface MGS in d-wave superconductors are robust features which result in a large number of observable effects: large Josephson current, low-temperature anomaly of the critical current, π-junction behaviour, $0 \rightarrow \pi$ junction crossover with temperature, zero-bias conductance peaks, paramagnetic currents, time reversal symmetry breaking and spontaneous interface currents, and resonance features in subgap currents.

Some of these consequences of MGS have been verified experimentally (ZBCP, paramagnetic currents and impurity-induced states), while some remain controversial (TRSB and spontaneous surface/interface currents), or so far unobserved (large Josephson current and the $1/T$ low-temperature anomaly of the critical current in low-transparency junctions).

A number of problems need to be clarified, for example the character and strength of relaxation processes and the width of the MGS. In particular, does the absence of MGS imply the absence of d-wave (and presence of s-wave), or does it imply d-wave and strong decoherence?

The predicted low-temperature anomaly associated with MGS, $I_c \propto 1/T$, remains to be confirmed experimentally. The lack of experimental evidence may be due to faceting of the GB (Hilgenkamp *et al* 1996): different parts of the junction may have local orientations supporting large MGS currents, but with opposite signs for different facets. Consequently, the low-temperature anomaly associated with the MGS may be averaged out for a macroscopic junction. The obvious remedy is to work with junctions with interfaces with well defined orientation.

The true nature of HTS GB and step-edge Josephson junctions remains, in our opinion, a mystery. It is difficult to get a consistent picture. In recent work on low-impedance step–edge junctions, a reasonable description of the Josephson current could be obtained assuming high transparency, while at the same time the low junction resistivity suggested that the transport is through high-transparency spots, point contacts or pinholes, in the interface barrier. In GB junctions at moderate misorientation angles a similar description may be appropriate. At large misorientation angles, however, the GB junctions have been characterized as a SIS tunnelling junctions with resonant states in the barrier. However, it is difficult to judge whether the experimental results imply coherent tunnelling or incoherent transport through the junction. Here, coevolution of experiment and theory seems to be necessary to obtain a deeper understanding.

Other predictions which need to be verified experimentally include negative differential conductance in sub-gap structures (needs a voltage-bias set-up), and spontaneous magnetization in TRSB states at $d_0/d_{\pi/4}$ junctions.

In a number of interesting recent experiments, a picture has emerged that the superconducting order parameter of the cuprates might not have pure $d_{x^2-y^2}$ symmetry but rather have a complex order parameter with $d_{x^2-y^2}+i\,d_{xy}$ symmetry, where the d_{xy} component is small compared to the $d_{x^2-y^2}$ component. STM studies of vortex cores in BSCCO (Pan *et al* 2000b) have revealed enhanced density of states at energies near ± 7 meV (i.e. well inside the bulk superconducting gap) with isotropic exponential dependence on distance from the core centre. This might indicate that a field induced $d_{x^2-y^2}+i\,d_{xy}$ order parameter is realized; see Franz and Tešanović (1998), Pan *et al* (2000b) and references therein. Tafuri and Kirtley (2000) have recently found spontaneous circulating currents around impurities in YBCO where the vortices contained fluxes of fractional size, in line with the idea of a complex order parameter induced near (magnetic) impurities (Graf *et al* 2000). Movshovich *et al* (1998) found that the thermal conductivity of nickel-doped BSCCO suddenly dropped at about 200 mK, which was taken as evidence for a second superconducting transition to a state with $d_{x^2-y^2}+i\,d_{xy}$ order. On the other hand, in a very recent experiment reported by Carmi *et al* (2000), spontaneous magnetization of *bulk* YBCO was found to appear at the superconducting transition temperature, meaning that the *bulk* order parameter may have complex $d_{x^2-y^2}+i\,d_{xy}$ symmetry. At this point, it seems crucial to collect more evidence for (or against) the $d_{x^2-y^2}+i\,d_{xy}$ order and establish whether it appears in the bulk at T_c, in magnetic fields, or near imperfections like magnetic impurities at low temperature.

Finally, the obvious, but perhaps naive, question concerns the all-important issue of the mechanism for high-T_c superconductivity, and the true symmetry of the order parameter. Despite the absence of definitive theory of the pairing mechanism and symmetry of the order parameter, a consistent picture of d-wave singlet pairing and Andreev MGS is slowly emerging, unifying a large body of experimental results and providing a framework for critical examination of present and future experiments. This means, perhaps, that inconsistent results may be discarded and significant new effects discovered and accepted. If another paradigm shift becomes unavoidable, e.g. based on a consistent non-Fermi-liquid picture of the normal state, it is likely that this must incorporate the present notion of Andreev MGS.

8. Note added in proof

Very recently new experimental data on the dc Josephson effect were reported, which give more evidence for the existence of MGS. Il'ichev *et al* (condmat/0102404) have studied the Josephson current-phase dependence in YBCO grain boundary junctions with $d_{\pi/8}/d_{-\pi/8}$ orientation. They observed a sign change of the first harmonic of the current along with an increase of the (negative) amplitude of the second current harmonic when the temperature decreases. This is an indication of the increasing contribution of MGS for $d_\alpha/d_{-\alpha}$ junctions as it is explained in section 3.2.3. In a paper published last year (Ovsyannikov *et al* 2000 *Vacuum* **58** 149) the $\sqrt{D}$-dependence of the critical current was observed at low temperature on YBCO grain boundary junctions with $\alpha_L = \alpha_R = 33^\circ$ orientation. The temperature dependence of the critical current below and above $T \sim 20$ K shows different behaviour, which is consistent with the discussion in section 3.2 of the role of MGS in such junctions, although it is not clear whether the low-temperature dependence of the critical

current obeys the $1/T$-law. These results are promising, but to make them more convincing further investigations of the angle-dependence of the Josephson current are desirable.

Acknowledgments

We are grateful to L Alff, M Fogelström, R Gross, I Iguchi, Z Ivanov, A Yurgens, J-X Zhu, and S Östlund for valuable discussions. We also thank T Claesson, C C Tsuei, and A Zagoskin for reading and commenting on the manuscript. Part of the studies included in the review was done during the visit of one of us (VS) to the Center for Advanced Studies in Oslo; VS is grateful to the administration of the Center and particularly to Yu Galperin for warm hospitality and support. This work has been supported by grants from NFR and NUTEK (Sweden) and NEDO (Japan).

Appendix A

In this appendix we provide a simple derivation of the MGS. In some detail, we first solve the BdG equation for bulk s-wave and d-wave superconductors and then we discuss the clean NS interface and the concept of Andreev reflection. The Andreev reflection phase shift used throughout the review is then obtained. Finally we show how the MGS are formed as a consequence of the sign difference between the lobes of the d-wave gap and why the formation of MGS is not sensitive to the detailed spatial dependence of the gap, although the MGS wavefunction itself depends on this shape.

Some particularly useful references regarding the technique used to obtain the solutions of the BdG equation for different structures can be found in Blonder *et al* (1982), Bruder (1990) and Bagwell (1992). For the s-wave NS junctions we refer to Blonder *et al* (1982) and for the d-wave case we refer to Bruder (1990). Bagwell (1992) derived the Andreev states present in s-wave SIS structures.

Appendix .1. Plane wave solutions of BdG equation

The BdG equations for s-wave superconductors are

$$\begin{cases} H_0 u(\boldsymbol{r}) + \Delta(\boldsymbol{r}) v(\boldsymbol{r}) = E u(\boldsymbol{r}) \\ -H_0 v(\boldsymbol{r}) + \Delta^*(\boldsymbol{r}) u(\boldsymbol{r}) = E v(\boldsymbol{r}) \end{cases} \tag{A.1}$$

where u and v are the electron and hole components of the wavefunction, $H_0 = -\hbar^2\nabla^2/2m - \mu$ in the simplest case, and E is measured relative to the chemical potential μ.

Equation (A.1) is easily solved for a bulk superconductor with $\Delta(\boldsymbol{r}) = \Delta =$ constant by making the following ansatz:

$$\Psi_S(\boldsymbol{r}) = \begin{pmatrix} u \\ v \end{pmatrix} \mathrm{e}^{\mathrm{i}\boldsymbol{k}\cdot\boldsymbol{r}} \tag{A.2}$$

where u and v do not depend on $\boldsymbol{r}$. The secular equation restricts the modulus of the $\boldsymbol{k}$ vectors, $\boldsymbol{k} = \boldsymbol{n}k$, to

$$k = \left(\frac{2m}{\hbar^2}(\mu \pm \sqrt{E^2 - \Delta^2})\right)^{1/2} \approx k_F \pm \frac{\xi}{\hbar v_F} \tag{A.3}$$

where $\xi = \sqrt{E^2 - \Delta^2}$. In the last step we assumed that the quasiparticle energy is much smaller than the Fermi energy. There will then be two types of wavefunctions, electron-like and hole-like, depending on what type of solutions they describe in the normal limit ($\Delta \to 0$). Labelling these as k^e and k^h, respectively, where $k^{e,h} = k_F \pm \sigma\xi/\hbar v_F$ ($\sigma = \operatorname{sgn} E$), we have

$$\Psi_S^e = \begin{pmatrix} u_0 \\ v_0 \end{pmatrix} \mathrm{e}^{\mathrm{i}k^e\boldsymbol{n}\cdot\boldsymbol{r}} \qquad \Psi_S^h = \begin{pmatrix} v_0 \\ u_0 \end{pmatrix} \mathrm{e}^{\mathrm{i}k^h\boldsymbol{n}\cdot\boldsymbol{r}} \tag{A.4}$$

where u_0 and v_0 are given by $v_0/u_0 = (E - \sigma\xi)/\Delta$ together with the normalization condition $|u_0|^2 + |v_0|^2 = 1$. Above we assumed that $|E| > \Delta$ since there cannot be any propagating solutions for energies below the gap. However, there are also exponentially decaying or growing solutions which become important for surfaces. By defining $\xi = \mathrm{i}\sigma\sqrt{\Delta^2 - E^2}$ for $|E| < \Delta$, the above expressions describe the exponentially decaying (in the direction of propagation) solutions for subgap energies.

For the normal metal, the solutions are obtained from the above by letting $\Delta \to 0$. The electron and hole wavefunctions can then be written as

$$\Psi_N^e = \begin{pmatrix} 1 \\ 0 \end{pmatrix} \mathrm{e}^{\mathrm{i}k_N^e\boldsymbol{n}\cdot\boldsymbol{r}} \qquad \Psi_N^h = \begin{pmatrix} 0 \\ 1 \end{pmatrix} \mathrm{e}^{\mathrm{i}k_N^h\boldsymbol{n}\cdot\boldsymbol{r}} \tag{A.5}$$

where $k_N^{e,h} \approx k_F \pm E/\hbar v_F$.

Note that the quasiparticle's direction of propagation is given by the group velocity $v_g = (1/\hbar)\,\mathrm{d}E/\mathrm{d}k$, which for a positive k is in the positive (negative) direction for electron-like (hole-like) quasiparticles.

Appendix .2. d-wave case

In the d-wave case, the BdG equations are non-local

$$\begin{cases} H_0 u(\boldsymbol{r}) + \displaystyle\int \mathrm{d}\boldsymbol{r}'\Delta(\boldsymbol{r}, \boldsymbol{r}')v(\boldsymbol{r}') = E u(\boldsymbol{r}) \\ -H_0 v(\boldsymbol{r}) + \displaystyle\int \mathrm{d}\boldsymbol{r}'\Delta^*(\boldsymbol{r}, \boldsymbol{r}')u(\boldsymbol{r}') = E v(\boldsymbol{r}). \end{cases} \tag{A.6}$$

Making the quasiclassical approximation as described in, for example, (Bruder 1990), we separate out the fast $1/k_F$ oscillations from the beginning by making the ansatz

$$\begin{pmatrix} u(\boldsymbol{r}) \\ v(\boldsymbol{r}) \end{pmatrix} = \begin{pmatrix} \tilde{u}(\boldsymbol{r}) \\ \tilde{v}(\boldsymbol{r}) \end{pmatrix} \mathrm{e}^{\mathrm{i}k_F\boldsymbol{n}\cdot\boldsymbol{r}} \tag{A.7}$$

where the spatially slowly varying envelope functions $\tilde{u}(\boldsymbol{r})$ and $\tilde{v}(\boldsymbol{r})$ satisfy the quasiclassical BdG equation

$$\begin{cases} -\mathrm{i}\hbar v_F \boldsymbol{n}\cdot\nabla\tilde{u}(\boldsymbol{r}) + \Delta(\boldsymbol{n}, \boldsymbol{r})\tilde{v}(\boldsymbol{r}) = E\tilde{u}(\boldsymbol{r}) \\ \mathrm{i}\hbar v_F \boldsymbol{n}\cdot\nabla\tilde{v}(\boldsymbol{r}) + \Delta^*(\boldsymbol{n}, \boldsymbol{r})\tilde{u}(\boldsymbol{r}) = E\tilde{v}(\boldsymbol{r}) \end{cases} \tag{A.8}$$

where terms of order $1/k_F\xi_0$ and higher have been neglected. This approximation is valid when the inequality $\Delta \ll E_F$ holds (see, for example, Andreev (1964)). For the spatially independent order parameter, taking the $\boldsymbol{r}$-dependence of $\tilde{u}(\boldsymbol{r})$ and $\tilde{v}(\boldsymbol{r})$ to be $\exp(\mathrm{i}\kappa(\boldsymbol{n})\boldsymbol{n}\cdot\boldsymbol{r})$, the secular equation restricts $\kappa(\boldsymbol{n})$ to $\pm\xi(\boldsymbol{n})/\hbar v_F$, where $\xi(\boldsymbol{n}) = \sqrt{E^2 - |\Delta(\boldsymbol{n})|^2}$. In the same way as in the s-wave case, we then find electron-like and hole-like solutions

$$\Psi_S^e = \begin{pmatrix} u_0 \\ v_0 \end{pmatrix} \mathrm{e}^{\mathrm{i}k^e\boldsymbol{n}\cdot\boldsymbol{r}} \qquad \Psi_S^h = \begin{pmatrix} v_0 \\ u_0 \end{pmatrix} \mathrm{e}^{\mathrm{i}k^h\boldsymbol{n}\cdot\boldsymbol{r}} \tag{A.9}$$

where $k^{e,h} = k_F \pm \sigma\xi(\boldsymbol{n})/\hbar v_F$, and u_0 and v_0 are given by $v_0/u_0 = (E - \sigma\xi(\boldsymbol{n}))/\Delta(\boldsymbol{n})$ together with the normalization condition $|u_0|^2 + |v_0|^2 = 1$.

As in the s-wave case, for subgap energies we can find exponentially growing or decaying solutions given by the above expressions if we let $\xi(\boldsymbol{n}) = \mathrm{i}\sigma\sqrt{|\Delta(\boldsymbol{n})|^2 - E^2}$.

Appendix .3. Andreev reflection

On a superconducting surface, electrons are reflected as holes and *vice versa*. In this section we will discuss this basic process more quantitatively by solving the BdG equation for the normal metal/s-wave superconductor interface. Putting the N/S interface at $x = 0$ and assuming that the gap depends on the space coordinate as

$$\Delta(x) = \begin{cases} 0 & x < 0 \\ \Delta \mathrm{e}^{\mathrm{i}\chi} & x > 0 \end{cases} \tag{A.10}$$

we are left with the simple problem of matching elementary plane wave solutions of the BdG equation in each region at the surface. The plane wave solutions of the BdG equation are derived above in this appendix. Assuming, for simplicity, propagation along the x-axis only, we write down an ansatz wavefunction describing an electron incident on the superconductor from the normal metal side

$$\Psi_N = \begin{pmatrix} 1 \\ 0 \end{pmatrix} \mathrm{e}^{\mathrm{i}k_N^e x} + A \begin{pmatrix} 0 \\ 1 \end{pmatrix} \mathrm{e}^{\mathrm{i}k_N^h x} + B \begin{pmatrix} 1 \\ 0 \end{pmatrix} \mathrm{e}^{-\mathrm{i}k_N^e x} \tag{A.11}$$

where we have taken into account that the electron may be reflected as an electron as well as a hole. On the superconductor side we include transmitted electron-like and hole-like quasiparticles

$$\Psi_S = C \begin{pmatrix} u_0 \\ v_0 \mathrm{e}^{-\mathrm{i}\chi} \end{pmatrix} \mathrm{e}^{\mathrm{i}k^e x} + D \begin{pmatrix} v_0 \\ u_0 \mathrm{e}^{-\mathrm{i}\chi} \end{pmatrix} \mathrm{e}^{-\mathrm{i}k^h x}. \tag{A.12}$$

At the interface (at $x = 0$) the wavefunction continuity gives

$$B = D = 0 \qquad C = 1/u_0 \qquad A = (v_0/u_0)\,\mathrm{e}^{-\mathrm{i}\chi}. \tag{A.13}$$

During this process of Andreev reflection, the electron incident from the normal metal is reflected as a hole with the probability amplitude A. The probability for Andreev reflection is $|A|^2 = 1$ for energies within the gap while quickly decreasing outside the gap. It is then convenient to write the amplitude of Andreev reflection for $|E| < \Delta$ of the form

$$A = \sigma \mathrm{e}^{-\mathrm{i}\gamma} \mathrm{e}^{-\mathrm{i}\chi} \qquad \gamma = \arccos\frac{E}{\Delta} \tag{A.14}$$

which defines the Andreev reflection phase shift γ used in the text. Note that the phase χ of Δ is also picked up during Andreev reflection. Charge conservation during Andreev reflection is preserved by letting a Cooper pair enter the superconductor. Consequently, a charge $2e$ is transferred from the normal metal to the superconductor, which explains how the subgap current may appear. In the same way, a hole incident on the superconductor from the normal metal side may be Andreev reflected as an electron transferring a charge $2e$ from the superconductor to the normal metal. The phase shift is in this case $-\gamma + \chi$ as can be checked by repeating the above calculation for an incident hole, keeping the rest of the ansatz as it is written.

Appendix .4. Midgap states

In this section we discuss quasiparticle reflection from the insulator/d-wave superconductor interface for energies within the superconducting gap and the formation of MGS. In the text we discussed MGS having the structure in figure 3 in mind. Here we show an alternative way of finding the MGS, in which it becomes clear that the normal metal plays no crucial role: the MGS is formed *only* as a consequence of the sign difference between the d-wave lobes. When the size of the normal metal in figure 3 becomes vanishingly small, the remaining part of the MGS wavefunction is the exponential tails in the superconductor. Here we study this wavefunction first for step-function shape of Δ and then for arbitrary shape.

Specular reflection at the surface imposes the following boundary condition for functions Ψ_S in equation (A.9): the eigenstate consists of a superposition of states with trajectories $\boldsymbol{n}$ and $\bar{\boldsymbol{n}}$, and the total wavefunction is zero at the surface, i.e.

$$\Psi_S(\boldsymbol{n}, 0) = -\Psi_S(\bar{\boldsymbol{n}}, 0). \tag{A.15}$$

For spatially constant Δ, the solutions of equation (A.8) with $E = 0$ and decaying at infinity are given by

$$\Psi_S(\boldsymbol{n}, \boldsymbol{r}) = \begin{pmatrix} 1 \\ \mathrm{i}\,\mathrm{sgn}\,\Delta \end{pmatrix} \mathrm{e}^{\mathrm{i}k_F \boldsymbol{n}\cdot\boldsymbol{r} - |\Delta/\hbar v_{Fx}|x}$$

$$\Psi_S(\bar{\boldsymbol{n}}, \boldsymbol{r}) = \begin{pmatrix} 1 \\ -\mathrm{i}\,\mathrm{sgn}\,\bar{\Delta} \end{pmatrix} \mathrm{e}^{\mathrm{i}k_F \bar{\boldsymbol{n}}\cdot\boldsymbol{r} - |\bar{\Delta}/\hbar v_{Fx}|x}. \tag{A.16}$$

If $\bar{\Delta} = -\Delta$, these functions have similar vector structure and they can be matched at the surface, $x = 0$, according to equation (A.15), and therefore there are MGS in this case.

Equation (A.8) has solutions at $E = 0$ also for arbitrary spatial variation of the gaps $\Delta(\boldsymbol{r})$ and $\bar{\Delta}(\boldsymbol{r})$. By introducing the following new variable,

$$\zeta = \int \mathrm{d}l |\Delta(l)|/\hbar v_F \tag{A.17}$$

where $l = \boldsymbol{n}\cdot\boldsymbol{r}$, one can reduce equation (A.8) to

$$\begin{cases} -\mathrm{i}\dfrac{\mathrm{d}\tilde{u}}{\mathrm{d}\zeta} + \mathrm{sgn}(\Delta)\tilde{v} = 0 \\ \mathrm{i}\dfrac{\mathrm{d}\tilde{v}}{\mathrm{d}\zeta} + \mathrm{sgn}(\Delta)\tilde{u} = 0. \end{cases} \tag{A.18}$$

These equations have solutions similar to those in equation (A.16), which leads to MGS.

References

Adagideli I, Goldbart P M, Shnirman A and Yazdani A 1999 *Phys. Rev. Lett.* **83** 5571

Alff L, Beck A, Gross R, Marx A, Kleefisch S, Bauch T, Sato H, Naito M and Koren G 1998a *Phys. Rev.* B **58** 11 197

Alff L and Gross R 1999 *Superlattices Microstruct.* **25** 1041

Alff L, Kleefisch S, Schoop U, Zittartz M, Kemen T, Bauch T, Marx A and Gross R 1998b *Eur. Phys. J.* B **5** 423

Alff L, Meyer S, Kleefisch S, Schoop U, Marx A, Sato H, Naito M and Gross R 1999 *Phys. Rev. Lett.* **83** 2644

Alff L, Takashima H, Kashiwaya S, Terada N, Ihara H, Tanaka Y, Koyanagi M and Kajimura K 1997 *Phys. Rev.* B **55** R14 757

Ambegokar V and Baratoff A 1963 *Phys. Rev. Lett.* **10** 593

Anderson P W 1966 *Phys. Rev. Lett.* **17** 95

Andreev A F 1964 *Zh. Eksp. Teor. Fiz.* **46** 1823 (Engl. Transl. 1964 *Sov. Phys.–JETP* **19** 1228)
——1965 *Zh. Eksp. Teor. Fiz.* **49** 655 (Engl. Transl. *Sov. Phys.–JETP* **22** 455)
Annett J, Goldenfeld N and Leggett A J 1996 *Physical Properties of High Temperature Superconductors* ed D M Ginsberg (Singapore: World Scientific)
Appelbaum J 1966 *Phys. Rev. Lett.* **17** 91
Aprili M, Badica E and Greene L H 1999 *Phys. Rev. Lett.* **83** 4630
Aprili M, Covington M, Paraoanu E, Niedermeier B and Greene L H 1998 *Phys. Rev.* B **57** R8139
Arie H, Yasuda K, Kobayashi H, Iguchi I, Tanaka Y and Kashiwaya S 2000 *Phys. Rev.* B **62** 11 864
Arnold G B 1987 *J. Low. Temp. Phys.* **68** 1
Artemenko S N, Volkov A F and Zaitsev A B 1979 *Zh. Eksp. Teor. Fiz.* **76** 1816 (Engl. Transl. 1979 *Sov. Phys.–JETP* **49** 924)
Ashcroft N W and Mermin N D 1976 *Solid State Physics* (Sunders College) p 367
Averin D and Bardas A 1995 *Phys. Rev. Lett.* **75** 1831
Bagwell P F 1992 *Phys. Rev.* B **46** 12 573
Balatsky A B and Salkola M I 1996 *Phys. Rev. Lett.* **76** 2386
Balatsky A B, Salkola M I and Rosengren A 1995 *Phys. Rev.* B **51** 15 547
Barash Y S 2000 *Phys. Rev.* B **61** 678
Barash Y S, Burkhardt H and Rainer D 1996 *Phys. Rev. Lett.* **77** 4070
Barash Y S, Galaktionov A V and Zaikin A D 1995 *Phys. Rev.* B **52** 665
Barash Y S, Kalenkov M S and Kurkijärvi J 2000 *Phys. Rev.* B **62** 6665
Barash Y S and Svidzinsky A A 1997 *Zh. Eksp. Teor. Fiz.* **111** 1120
Barash Y S, Svidzinsky A A and Burkhardt H 1997 *Phys. Rev.* B **55** 15 282
Bardeen J 1961 *Phys. Rev. Lett.* **6** 57
Bardeen J and Johnson J L 1972 *Phys. Rev.* B **5** 72
Bednorz G and Müller K A 1986 *Z. Phys.* B **64** 189
Beenakker C W J 1991 *Phys. Rev. Lett.* **67** 3836
Beenakker C W J and van Houten H 1991 *Single Electron Tunneling and Mesoscopic Devices* (Berlin: Springer)
Behnia K, Belin S, Aubin H, Rullier-Albenque F, Ooi S, Tamegai T, Deluzet A and Batail P 1999 *J. Low Temp. Phys.* **117** 1089
Blonder G E, Tinkham M and Klapwijk T M 1982 *Phys. Rev.* B **25** 4515
Bratus' E N, Shumeiko V S, Bezuglyi E V and Wendin G 1997 *Phys. Rev.* B **55** 12 666
Bratus' E N, Shumeiko V S and Wendin G 1995 *Phys. Rev. Lett.* **74** 2110
Bruder C 1990 *Phys. Rev.* B **41** 4017
Buchholtz L J, Palumbo M, Rainer D and Sauls J A 1995a *J. Low. Temp. Phys.* **101** 1079
——1995b *J. Low. Temp. Phys.* **101** 1099
Buchholtz L J and Zwicknagl G 1981 *Phys. Rev.* B **23** 5788
Büttiker M 1986 *Phys. Rev. Lett.* **57** 1761
Carmi R, Polturak E, Koren G and Auerbach A 2000 *Nature* **404** 853
Carrington A, Manzano F, Prozorov R, Giannetta R W, Kameda N and Tamegai T 2001 *Phys. Rev. Lett.* **86** 1074
Cohen M H, Falicov L M and Phillips J C 1962 *Phys. Rev. Lett.* **8** 316
Covington M, Aprili M, Paraoanu E, Greene L H, Xu F, Zhu J and Mirkin C A 1997 *Phys. Rev. Lett.* **79** 277
Covington M and Greene L H 2000 *Phys. Rev.* B **62** 12 440
Cuevas J C, Martin-Rodero A and Levy-Yeyati A 1996 *Phys. Rev.* B **54** 7366
Dagotto R 1994 *Rev. Mod. Phys.* **66** 763
de Gennes P G 1989 *Superconductivity of Metals and Alloys* (Advanced Books Classics)
de Gennes P G and Saint-James D 1963 *Phys. Lett.* **4** 151
Delin K A and Kleinsasser A W 1996 *Supercond. Sci. Technol.* **9** 227
Early E A, Clark A F and Char K 1993 *Appl. Phys. Lett.* **62** 3357
Ekin J W, Xu Y, Mao S, Venkatesan T, Face D W, Eddy M and Wolf S A 1997 *Phys. Rev.* B **56** 13 746
Estève D, Martinis J M, Urbina C, Devoret M H, Collin G, Monod P, Ribault M and Revcolevschi A 1987 *Europhys. Lett.* **3** 1237
Flatté M E and Byers J M 1998 *Phys. Rev. Lett.* **80** 4546
Fogelström M, Rainer D and Sauls J A 1997 *Phys. Rev. Lett.* **79** 281
Fogelström M and Yip S K 1998 *Phys. Rev.* B **57** R14 060
Fogelström M, Yip S K and Kurkijärvi J 1998 *Physica* C **294** 289
Franz M and Tešanović Z 1998 *Phys. Rev. Lett.* **80** 4763
Geerk J, Xi X X and Linker G 1988 *Z. Phys.* B **73** 329
Geshkenbein V B, Larkin A I and Barone A 1987 *Phys. Rev.* B **36** 235
Giaever I 1960 *Phys. Rev. Lett.* **5** 147
Golubov A A and Kupriyanov M Y 1999 *Superlattices Microstruct.* **25** 949
Graf M J, Balatsky A V and Sauls J A 2000 *Phys. Rev.* B **61** 3255
Gross R 1994 *Interfaces in High-T_c Superconducting Systems* (New York: Springer) ch 6, p 176
Haas S and Maki K 2000 *Phys. Rev. Lett.* **85** 2172
Higashitani S 1997 *J. Phys. Soc. Japan* **66** 2556
Hilgenkamp H, Mannhart J and Mayer B 1996 *Phys. Rev.* B **53** 14 586
Honerkamp C and Sigrist M 1999 *Physica* C **317–18** 489
Honerkamp C, Wakabayashi K and Sigrist M 2000 *Europhys. Lett.* **50** 368
Hu C R 1994 *Phys. Rev. Lett.* **72** 1526
——1998 *Phys. Rev.* B **57** 1266
Huck A, van Otterlo A and Sigrist M 1997 *Phys. Rev.* B **56** 14 163
Hudson E W, Pan S H, Gupta A K, Ng K W and Davis J C 1999 *Science* **285** 88
Hulm J K 1953 *Phys. Rev.* **90** 1116
Hurd M 1997 *Phys. Rev.* B **55** R11 993
Hurd M, Löfwander T, Johansson G and Wendin G 1999 *Phys. Rev.* B **59** 4412
Hussey N E, Beknia K, Takagi H, Urano C, Adachi S and Tajima S 2000 *Preprint* cond-mat/0004094
Iguchi I, Wang W, Yamazaki M, Tanaka Y and Kashiwaya S 2000 *Phys. Rev.* B **62** R6131
Ilichev E, Zakosarenko V, IJsselsteijn R P J, Hoenig H E, Schultze V, Meyer H G, Grajcar M and Hlubina R 1999 *Phys. Rev.* B **60** 3096
Imry Y 1986 *Directions in Condensed Matter Physics* ed G Grinstein and G Mazenko (Singapore: World Scientific) p 101
Ivanov Z G, Stepantsov E A, Claesson T, Wenger F, Lin S Y, Khare N and Chaudhari P 1998 *Phys. Rev.* B **57** 602
Johansson G, Bratus' E N, Shumeiko V S and Wendin G 1999b *Phys. Rev.* B **60** 1382
Johansson G, Wendin G, Bratus' E N and Shumeiko V S 1999a *Superlattices Microstruct.* **25** 905
Josephson B D 1962 *Phys. Lett.* **1** 251
Kashiwaya S, Ito T, Oka K, Ueno S, Takashima H, Koyanagi M, Tanaka Y and Kajimura K 1998a *Phys. Rev.* B **57** 8680
Kashiwaya S, Tanaka Y, Terada N, Koyanagi M, Ueno S, Alff L, Takashima H, Tanuma Y and Kajimura K 1998b *J. Phys. Chem. Sol.* **59** 2034
Kashiwaya S and Tanaka Y 1996 *Phys. Rev.* B **53** 2667
——1999 *Superlattices Microstruct.* **25** 1099
——2000 *Rep. Prog. Phys.* **63** 1641
Kashiwaya S, Tanaka Y, Koyanagi M, Takashima H and Kajumura K 1995 *Phys. Rev.* B **51** 1350
Kirtley J R, Chaudhari P, Ketchen M B, Khare N, Lin S Y and Shaw T 1995a *Phys. Rev.* B **51** R12 057
Kirtley J R, Tsuei C C, Rupp M, Sun J Z, Yu-Jahnes L S, Gupta A and Ketchen M B 1996 *Phys. Rev. Lett.* **76** 1336
Kirtley J R, Tsuei C C, Sun J Z, Chi C C, Yu-Jahnes L S, Gupta A, Rupp M and Ketchen M B 1995b *Nature* **373** 225
Klapwijk T M, Blonder G E and Tinkham M 1982 *Physica* B **109–110** 1657
Kleefisch S, Alff L, Schoop U, Marx A and Gross R 1998 *Appl. Phys. Lett.* **72** 2888
Kleiner R *et al* 1996 *Phys. Rev. Lett.* **76** 2161
Kouznetsov K A *et al* 1997 *Phys. Rev. Lett.* **79** 3050
Krupke R and Deutscher G 1999 *Phys. Rev. Lett.* **83** 4634
Kulik I O 1969 *Zh. Eksp. Teor. Fiz.* **57** 1745 (Engl. Transl. 1970 *Sov. Phys.–JETP* **30** 944)

Landauer R 1957 *IBM J. Res. Dev.* **1** 223
Lesueur J, Aprili M, Goualan A, Horton T J and Dumoulin L 1997 *Phys. Rev.* B **55** 3398
Lesueur J, Grison X, Aprili M and Kontos T 1999 *J. Low. Temp. Phys.* **117** 539
Löfwander T, Johansson G, Hurd M and Wendin G 1998 *Phys. Rev.* B **57** R3225
Löfwander T, Johansson G, Shumeiko V, Wendin G and Hurd M 1999a *Superlattices Microstruct.* **25** 1115
Löfwander T, Johansson G and Wendin G 1999b *J. Low. Temp. Phys.* **117** 593
Löfwander T, Shumeiko V S and Wendin W 2000 *Phys. Rev.* B **62** R14 653
Ludoph B, van der Post N, Bratus' E N, Bezuglyi E V, Shumeiko V S, Wendin G and van Ruitenbeek J 2000 *Phys. Rev.* B **61** 856
Mannhart J, Hilgenkamp H, Mayer B, Gerber C, Kirtley J R, Moler K A and Sigrist M 1996a *Phys. Rev. Lett.* **77** 2782
Mannhart J, Mayer B and Hilgenkamp H 1996b *Z. Phys.* B **101** 175
Mathai A, Gim Y, Black R C, Amar A and Wellstood F C 1995 *Phys. Rev. Lett.* **74** 4523
Matsumoto M, Kaneko S and Nishida N 1997 *J. Phys. Soc. Japan* **66** 3211
Matsumoto M and Shiba H 1995a *J. Phys. Soc. Japan* **64** 3384
——1995b *J. Phys. Soc. Japan* **64** 4867
——1995c *J. Phys. Soc. Japan* **64** 1703
——1996 *J. Phys. Soc. Japan* **65** 2194
Melsen J A, Brouwer P W, Frahm K M and Beenakker C W J 1996 *Europhys. Lett.* **35** 7
Mendelssohn K and Olsen J L 1950 *Phys. Rev.* **80** 859
Mössle M and Kleiner R 1999 *Phys. Rev.* B **59** 4486
Movshovich R, Hubbard M A, Salamon M B, Balatsky A V, Yoshizaki R, Sarrao J L and Jaime M 1998 *Phys. Rev. Lett.* **80** 1968
Nagato Y and Nagai K 1995 *Phys. Rev.* B **51** 16 254
Östlund S 1998 *Phys. Rev.* B **58** R14 757
Pan S H, Hudson E W, Gupta A K, Ng K W, Eisaki H, Uchida S and Davis J C 2000b *Phys. Rev. Lett.* **85** 1536
Pan S H, Hudson E W, Lang K M, Eisaki H, Uchida S and Davis C J 2000a *Nature* **403** 746
Poenicke A, Barash Y S, Bruder C and Istyukov V 1999 *Phys. Rev.* B **59** 7102
Prozorov R, Giannetta R W, Fournier P and Greene R L 2000 *Phys. Rev. Lett.* **85** 3700
Rae A I M 2000 *Phys. Rev. Lett.* **84** 2235
Riedel R A and Bagwell P F 1998 *Phys. Rev.* B **57** 6084
Salkola M I, Balatsky A B and Scalapino D J 1996 *Phys. Rev. Lett.* **77** 1841
Samanta M P and Datta S 1998 *Phys. Rev.* B **57** 10 972
Samuelsson P, Lantz J, Shumeiko V S and Wendin G 2000 *Phys. Rev.* B **62** 1319
Scalapino D J 1995 *Phys. Rep.* **250** 330
Schrieffer J R and Wilkins J W 1963 *Phys. Rev. Lett.* **10** 17
Schulz R R, Chesca B, Goetz B, Schneider C W, Schmehl A, Bielefeldt H, Hilgenkamp H, Mannhart J and Tsuei C C 2000 *Appl. Phys. Lett.* **76** 912
Shumeiko V S, Bratus' E N and Wendin G 1997 *Low. Temp. Phys.* **23** 181
Sigrist M 1998 *Prog. Theor. Phys.* **99** 899
Sigrist M, Bailey D B and Laughlin R B 1995 *Phys. Rev. Lett.* **74** 3249
Sigrist M and Rice T M 1995 *Rev. Mod. Phys.* **67** 503
Sinha S and Ng K W 1998 *Phys. Rev. Lett.* **80** 1296
Strässler S and Wyder P 1963 *Phys. Rev. Lett.* **10** 225
Sun A G, Gajewski D A, Maple M B and Dynes R C 1994 *Phys. Rev. Lett.* **72** 2267
Suzuki K, Ichimura K, Nomura K and Takekawa S 1999 *Phys. Rev. Lett.* **83** 616
Tafuri F and Kirtley J R 2000 *Phys. Rev.* B **62** 13 934
Tafuri F, Miletto Granozio F, Carillo F, Di Chiara A, Verbist K and Van Tendeloo G 1999 *Phys. Rev.* B **59** 11 523
Taillefer L, Lussier B, Gagnon R, Behnia K and Aubin H 1997 *Phys. Rev. Lett.* **79** 483
Tanaka Y and Kashiwaya S 1995 *Phys. Rev. Lett.* **74** 3451
——1996a *Phys. Rev.* B **53** R11 957
——1996b *Phys. Rev.* B **53** 9371
——1997 *Phys. Rev.* B **56** 892
——1998 *Phys. Rev.* B **58** R2948
——1999 *Superlattices Microstruct.* **25** 1083
Tanuma Y, Tanaka Y, Ogata M and Kashiwaya S 1999 *Phys. Rev.* B **60** 9817
Tsuei C C and Kirtley J R 2000a *Rev. Mod. Phys.* **72** 969
——2000b *Phys. Rev. Lett.* **85** 182
Tsuei C C, Kirtley J R, Chi C C, Yu-Jahnes L S, Gupta A, Shaw T, Sun J Z and Ketchen M B 1994 *Phys. Rev. Lett.* **73** 593
Tsuei C C, Kirtley J R, Ren Z F, Wang J H, Raffy H and Li Z Z 1997 *Nature* **387** 481
Tsuei C C, Kirtley J R, Rupp M, Sun J Z, Gupta A, Ketchen M B, Wang C A, Ren Z F, Wang J H and Bhushan M 1996 *Science* **271** 329
van Harlingen D J 1995 *Rev. Mod. Phys.* **67** 515
Vollhardt D and Wölfle P 1990 *The Superfluid Phases of Helium-3* (London: Taylor and Francis)
Walker M P and Pairor P 1999 *Phys. Rev.* B **60** 10 395
Walter H, Prusseit W, Semerad R, Kinder H, Assmann W, Huber H, Burkhardt H, Rainer D and Sauls J A 1998 *Phys. Rev. Lett.* **80** 3598
Wang W, Yamazaki M, Lee K and Iguchi I 1999 *Phys. Rev.* B **60** 4272
Wei J Y T, Yeh N C, Garrigus D F and Strasik M 1998 *Phys. Rev. Lett.* **81** 2542
Wendin G and Shumeiko V S 1996a *Phys. Rev.* B **53** R6006
——1996b *Superlattices Microstruct.* **20** 569
Wolf E L 1985 *Principles of Electron Tunneling Spectroscopy* (Oxford: Oxford University Press)
Wollman D A, Harlingen D J V, Giapinzakis J and Ginsberg D M 1995 *Phys. Rev. Lett.* **74** 797
Wollman D A, Harlingen D J V, Lee W C, Ginsberg D M and Leggett A J 1993 *Phys. Rev. Lett.* **71** 2134
Xu J H, Miller J H Jr and Ting C S 1996 *Phys. Rev.* B **53** 3604
Yazdani A, Howald C M, Lutz C P, Kapitulnik A and Eigler D M 1999 *Phys. Rev. Lett.* **83** 176
Yeh N C, Fu C C, Chen C T, Huang Z, Vasquez R P and Tajima S 2000 *Superconducting and Related Oxides: Physics and Nanoengineering IV* ed D Pavuna and I Bosovic *Proc. SPIE* **4058** 60
Yip S K 1993 *J. Low. Temp. Phys.* **91** 203
——1995 *Phys. Rev.* B **52** 3087
——1997 *J. Low. Temp. Phys.* **109** 547
Yip S K, de Alcantara Bonfim O F and Kumar P 1990 *Phys. Rev.* B **41** 11 214
Yoshida N, Tanaka Y and Kashiwaya S 1999 *Physica* C **317–318** 666
Zagoskin A M and Oshikawa M 1998 *J. Phys.: Condens. Matter* **10** L105
Zagoskin M 1997 *J. Phys.: Condens. Matter* **9** L419
Zavaritsky N 1960 *Zh. Eksp. Teor. Fiz.* **38** 1672 (Engl. Transl. 1960 *Sov. Phys.–JETP* **11** 1207)
Zhu J X, Friedman B and Ting C S 1999 *Phys. Rev.* B **60** R3739
Zhu J X, Lee T K, Ting C S and Hu C R 2000a *Phys. Rev.* B **61** 8667
Zhu J X, Sheng D N and Ting C S 2000c *Preprint* cond-mat/0005266
Zhu J X, Ting C S and Hu C R 2000b *Phys. Rev.* B **62** 6027